TRIBHUVAN UNIVERSITY
INSTITUTE OF ENGINEERING
PULCHOWK CAMPUS

THESIS NO.:

Analysis of Conjugate Natural Convection Inside a Partitioned Differentially Heated Enclosure

by

Balaram Kushwaha

A THESIS
SUBMITTED TO DEPARTMENT OF MECHANICAL AND AEROSPACE ENGINEERING IN PARTIAL FULFILLMENT OF THE REQUIREMENT FOR THE DEGREE OF MASTER OF SCIENCE IN
MECHANICAL SYSTEMS DESIGN AND ENGINEERING

DEPARTMENT OF MECHANICAL AND AEROSPACE ENGINEERING
LALITPUR, NEPAL

MARCH, 2022

COPYRIGHT

TRIBHUVAN UNIVERSITY

INSTITUTE OF ENGINEERING

PULCHOWK CAMPUS

DEPARTMENT OF MECHANICAL AND AEROSPACE ENGINEERING

The undersigned certify that they have read, and recommend to the Institute of Engineering for acceptance, a thesis entitled "**Analysis of Conjugate Natural Convection Inside a Partitioned Differentially Heated Enclosure**" submitted by Balaram Kushwaha in partial fulfillment of the requirements for the degree of Master in Mechanical Systems Design and Engineering.

_____

Supervisor, Asso. Prof. Dr. Hari Bahadur Darlami
Asso. Professor, Department of Mechanical and Aerospace Engineering, Pulchowk Campus

_____

Supervisor, Asst. Prof. Kamal Darlami
Asst. Professor, Department of Mechanical and Aerospace Engineering, Pulchowk Campus

_____

External Examiner, Prof. Dr. Bivek Baral
Professor, Department of Mechanical Engineering
Kathmandu University

_____

Committee Chairperson, Dr. Surya Prasad Adhikari
Head, Department of Mechanical and Aerospace Engineering, Pulchowk Campus

Date: 20th March, 2022

ABSTRACT

Inside a differentially heated cavity, a numerical study of conjugate natural convection is carried out. In this work, two separate situations are investigated: an enclosure with a wavy partition filled with heat generating fluid and an enclosure with a solid partition splitting the cavity into two different fluid zones, namely air and water. Two-dimensional continuity, momentum, and energy equations regulate thermal and flow properties inside the cavity. Numerical analysis for the wavy partitioned enclosure is performed over varying external *Ra* ($10^3 \leq Ra_{ae} \leq 10^8$), various position of the wavy partition wall ($X_p = 0.25L$, $0.50L$ and $0.75L$), different frequencies of the wavy partition wall (f = 6, 9 and 12), and three varying thermal conductivity ratios. Similarly, numerical analysis over a varying range of Rayleigh number ($10^3 \leq Ra_a \leq 10^6$), various thickness of solid partition wall ($0.05L \leq \varepsilon \leq 0.2L$), various location ($0.25L \leq c \leq 0.75L$), and various thermal conductivity of the wall. The influences of the above governing parameters on the streamline and the isotherm plots are examined. Furthermore, the effect of partition wall thickness, location, and thermal conductivity on the *Nu* of hot and cold walls is estimated in the current study. The results suggest that increasing the thermal conductivity of the wall material enhances thermal exchange performance, whereas changing the position of the wavy partition wall has less of an impact. Heat transmission, however, reduces when the frequency of waviness increases. In the second scenario, the results show that increasing the wall material's thermal conductivity enhances heat transmission performance. Heat transmission is reduced when the thickness and distance of the partition wall from the cold end are increased. Similarly, a comparative analysis of the thermal exchange performance between the solid and wavy partitioned enclosure with and without the heat generating fluid is also analyzed in this study. Thermal exchange characteristics improved by nearly 8% and 15% for wavy partitioned enclosure at high Rayleigh number corresponding to enclosure filled without and with heat generating fluid respectively.

ACKNOWLEDGEMENTS

I would like to express my profound appreciation and sincere thanks to Asso. Prof. Dr. Hari Bahadur Darlami and Asst. Prof. Kamal Darlami, my thesis supervisors, for their professional advice, constant support and recommendations when required, and unwavering encouragement during the research period.

I would also want to thank the Department of Mechanical and Aerospace Engineering, as well as the Institute of Engineering, for their help with the thesis. Dr. Surya Prasad Adhikari, Head of Department of Mechanical and Aerospace Engineering, Pulchowk Campus, has my gratitude for his assistance and advice. I would like to thank Prof. Dr. Laxman Poudel, MSMDE coordinator, for building an amazing interactive environment for thesis work, as well as the complete elite committee members for their helpful remarks and advice that helped to make this work more relevant. I would also want to thank every one of my 075MSMDE coworkers for their constant support, thoughts, and recommendations.

I would want to use this time to offer my heartfelt gratitude and appreciation to my family members for their unwavering support and constant source of inspiration during this thesis project.

TABLE OF CONTENTS

LIST OF TABLES

LIST OF FIGURES

NOMENCLATURE OF SYMBOLS

a_r	:	Aspect Ratio, H / L
L	:	Length
H	:	Height
$c_{p,a}$	:	Specific heat of air at constant pressure
$c_{p,w}$	:	Specific heat of water at constant pressure
g	:	Acceleration due to gravity
k	:	Thermal conductivity
k_a	:	Thermal conductivity of air
k_w	:	Thermal conductivity of water
k_r	:	Thermal conductivity ratio, $k_r = k_s / k_a$
k_s	:	Thermal conductivity of wall
Nu_H	:	Nusselt number along hot wall
Nu_C	:	Nusselt number along cold wall
Pr_a	:	Prandtl number of air
Pr_w	:	Prandtl number of water
Ra_a	:	Rayleigh number of air
Ra_{ai}	:	Internal Rayleigh number of air
Ra_{ae}	:	External Rayleigh number of air
Ra_w	:	Rayleigh number of water
Gr_a	:	Grashof number of air
Θ_{av}	:	Average temperature
$\Theta_{av,a}$	:	Fluid temperature of air domain
$\Theta_{ag,w}$	:	Fluid temperature of water domain
T	:	Dimensional temperature
T_H	:	Temperature of heated wall
T_C	:	Temperature of cold wall
u	:	x-axis velocity
v	:	y-axis velocity
x	:	x-Cartesian coordinate
y	:	y-Cartesian coordinate

p	:	Fluid pressure
U	:	Non-dimensional x-axis velocity
V	:	Non-dimensional y-axis velocity
X	:	Non-dimensional horizontal axis
Y	:	Non-dimensional vertical axis
P	:	Non-dimensional fluid pressure
α_a	:	Thermal diffusivity of air
β	:	Thermal expansion coefficient
Θ	:	Non-dimensional fluid temperature
ν_a	:	Kinematic viscosity of air
μ_a	:	Dynamic viscosity of air
μ_w	:	Dynamic viscosity of water
ρ_a	:	Density of air
ρ_w	:	Density of water
ε	:	Thickness of the solid partition
c	:	Position of the solid partition
T_p	:	Thickness of the wavy partition
X_p	:	Position of the wavy partition

LIST OF ACRONYMS AND ABBREVIATIONS

CFD	:	Computational Fluid Dynamics
FEM	:	Finite Element Method
LMTD	:	Log Mean Temperature Difference

CHAPTER ONE: INTRODUCTION

1.1 Background

Conduction is dominant for the thermal exchange in solids whereas convection usually dominates in fluids. Conjugate thermal exchange is observed in many situations that includes wall cavities, solar collector, cryogenic chambers etc. For instance, heat sinks are made efficient by combining thermal exchange by conduction in the heat sink with the convection in the surrounding fluids.

The conjugate thermal exchange method has become an important tool for designing and studying various engineering and natural phenomena. The wide ranges of its application encompass food processing, thermal insulation, heat exchangers etc.

Free convection inside an enclosure is frequently encountered in practice. The fluid in touch with the heated surface rises and the fluid in contact with the cold surface falls in a vertical cavity, causing a rotating motion of fluid inside the cavity and improving heat transmission. Similarly, the heat transmission parameters of a horizontal enclosure are determined by the location of the heated surface. When a hot surface is layered on top of a cold surface, the fluid next to the hot surface warms up but cannot ascend upwards, resulting in no fluid motion. In this situation, heat is transferred solely by conduction. When a hot surface is put at the bottom of a container, heated fluid with a low density rises and is replaced by cold heavy fluid. As a result, a current of fluid motion is created, resulting in increased heat transmission. The cavity walls are differentially heated and the partition wall divides the cavity into two separate domains. The partition wall has a definite thermal conductivity and thermal exchange across the partition wall occurs through conduction. Thermal exchange in the separate domains occurs mainly due to convection combined with conduction thermal exchange in the partition results in conjugate natural convection. Introduction of partition inside a cavity has found many applications in recent days owing to the reduced thermal exchange. Solar collectors, energy saving and thermal insulation of dwellings, double pane windows, and other applications demonstrate the relevance natural convection.

The research of rapid and increased cooling of tiny devices such as laptops and smart phones that incorporate nano- and micro-electronic processors is gaining traction as the

popularity of these devices grows. Furthermore, in recent years, academics have been more motivated to discover new ways for improving thermal exchange equipment that are less expensive to manufacture and run, as well as conserve resources and energy. Automobile and spaceship cooling systems, as well as heat exchangers in air conditioning and refrigeration systems, must be as small and light as feasible. Furthermore, they are commonly used to provide efficient heat transmission and energy conservation by reducing heat losses.

1.2 Problem statement

Rapid technological advancements have increased the need for efficient heat transport. One of the main goals of these recent studies is to gain an understanding of convection in enclosures that are used in modern engineering. Natural convection inside an enclosure that is combined is a topic of great significance. Thermal exchange in a partitioned cavity has received a lot of attention in recent years as a fundamental thermal exchange process. The majority of researchers have looked into a solid divider installed inside the container. However, there have been few researches on the effect of wavy partitions on thermal and flow characteristics inside an enclosure, which are explored further in the literature review. The insufficient research done in this aspect inspired this research topic. Numerical simulations for accessing the effect of wavy partition wall inside the enclosure are carried out in this study.

Moreover, only few investigations have been performed to analyze the thermal exchange inside an enclosure divided by solid partition into two fluid zones. The considerations made by some researchers had limitations and this present study intends to overcome those.

1.3 Objectives

The main objective of this thesis is to perform analysis of the thermal and flow characteristic in a wavy and solid partitioned enclosure.

The specific objectives of the present research are as follows:

- To analyze the impact of variation of thickness, position and material of the solid partition on thermal exchange inside a partitioned square enclosure filled with different fluids in each cavity

- To analyze the impact of variation of position, frequency and material of the wavy partition on thermal exchange characteristic inside a partitioned cavity filled with heat generating fluid

- To compare the thermal and flow performance between the differentially heated enclosure with wavy and solid partition

- To analyze the application on a double and triple pane window and make a comparative analysis

1.4 Assumptions and limitations

- The internal Rayleigh number of the heat generating fluid inside the enclosure is assumed to be constant and a low value of the internal Rayleigh number is assumed for the study
- Only a computational examination is analyzed to access the thermal and flow performance in an enclosure

CHAPTER TWO: LITERATURE REVIEW

The characteristics of conjugate natural convection inside partitioned enclosed cavities are being studied over the past 30 years. Anderson & Bejan (1981) investigated heat exchange in an enclosure both theoretically and empirically at first. In order to measure thermal performance, they employed water to produce a higher *Ra* in a scaled-down container with various partitions. Since then, numerous researchers have been interested in studying the thermal performance of partitioned cavities. For changing *Ra*, Kahveci (2007a), Kahveci (2007b),Kahveci & Öztuna (2008), Salama et al. (2014), Khatamifar et al. (2017), Acharya & Tsang (1985) , Tong & Gerner (1986), Ho & Yih (1987), and Kangni et al. (1991) employed air and explored the impacts of inserting partition(s) within an enclosure. The thermal performance of an enclosure with a central partition was explored by Acharya & Tsang (1985). The highest *Nu* along the hot (cold) surface was found in the center position of the partition, according to the results. Tong & Gerner (1986) and Ho & Yih (1987) used a finite difference approach to investigate thermal properties in a rectangular enclosure and found that an enclosure with a partition had a worse thermal performance. Kangni et al. (1991) explored heat exchange in multiple partitioned enclosures, building on prior research. They investigated the impacts of several partitions in a cavity using a finite difference formulation and a volume control approach, and found that as the number of partitions increased, the thermal performance decreased. Similarly, Kahveci (2007a) and Kahveci (2007b) statistically examined heat performance in partitioned enclosures, finding that the average Nusselt number drops. Finally, Khatamifar et al. (2017) investigated the effects of the partition's aspect ratio, *Ra*, location, thickness, and thermal conductivity on thermal performance in a square cavity and discovered that the heated *Nu* rises as *Ra* increases.

Many researchers are interested in the influence of employing water as a working fluid on conjugate natural thermal performance. Anderson & Bejan (1981), Nishimura et al. (1988), Xu et al. (2009), Saha et al. (2015), and Williamson et al. (2012) all looked at cavities filled with fluid other than air. Using a wavy conducting partition in a square hollow filled with water and altering the amplitude of the wall with a constant frequency, Saha et al. (2015) conducted research. Similarly, Xu et al. (2009)

quantitatively examined and categorized natural convection flow development into three stages: early, transitional, and constant. For their research, Nishimura et al. (1988) and Williamson et al. (2012) employed fluids other than air and water with $Pr_a > 1$. Nishimura et al. (1988) investigated the impact of many partitions in a water-filled rectangular hollow with differently heated side walls both experimentally and statistically, and established a relationship between *Nu* and Ra_{ae}, aspect ratio, and partition number. According to their research, utilizing a 2-5 partition can limit heat exchange by 70 to 90%.

Nishimura et al. (1988)explored the influence of various partitions on conjugate natural convection thermal exchange rate within a differentially heated cavity. Anderson & Bejan (1981), Kangni et al. (1991); Nishimura et al. (1988). concluded that the net thermal exchange rate changed inversely with (1+n), where n is the number of vertical partitions, according to their findings. Finally, they conducted experiments to confirm their conclusions. Acharya & Tsang (1985); Ho & Yih (1987); Kahveci & Öztuna (2008); Kangni et al. (1991); Tong & Gerner (1986) and Williamson et al. (2012) investigated the influence of aspect ratio on conjugate natural convection within partitioned cavities. Their findings revealed that a lower aspect ratio led to higher viscous resistance and lower flow velocities. They also discovered that as the aspect ratio is increased, the Nusselt number decreases. Kahveci (2007a), (2007b); Kahveci & Öztuna (2008); Kangni et al. (1991); Oztop et al. (2009) and Varol et al. (2010) investigated the effect of thermal conductivity of the partition on thermal exchange characteristics and discovered that as the thermal resistance of the partition decreases, the average Nusselt number increases to a peak, and as the thermal resistance decreases.

Apart from studies on conjugate natural convection, Cuckovic-Dzodzo et al. (1999) and Kahveci & Öztuna (2008) studied the effect of *Pr* on conjugate natural convection inside a partitioned differentially heated cavity, and found that Prandtl number has little effect on fluid flow and thermal exchange. Cuckovic-Dzodzo et al. (1999); Ghosh et al. (1992) and Turkoglu & Yücel (1996), on the other hand, investigated the influence of aspect ratio on conjugate natural convection within a partitioned cavity filled with a working fluid other than air or water. Ghosh et al. (1992) found that the position of the partition affects flow by generating lower driving force in separated convection systems and reducing heat exchange compared to a cavity without partition for low aspect ratios.

Cuckovic-Dzodzo et al. (1999) created a relationship that represents the inverse relationship between average Nusselt number and cavity aspect ratio.

Acharya (1985) investigated natural convection in an inclined enclosure with internal energy sources using the finite difference method. Rayleigh numbers up to 10^6, as well as inclination angles of 30° to 60°, were examined. When the internal Rayleigh number was more than the external Rayleigh number, the flow climbed within the enclosure and went down for both the hot and cold walls, however when the external Rayleigh number was considerable, the flow flowed upward for the hot wall and downward for the cold wall. Similarly, the average heat flow ratio rose as the external Rayleigh number grew and the inner Rayleigh number fell.

Fusegi et al. (1991). quantified natural convection in a differentially heated square cavity with uniform internal heat generation. The Rayleigh number on the inside was modified from 10^9 to 10^{10}, however the Rayleigh number on the outside stayed at 5×10^7. As the strength of internal generation increased, the flow at the top component of the hot wall was directed downwards, and thermal energy escaped from the system to the surrounding from the hot wall's over-the-top area. To convey heat into the system, just the lowest part of the heated wall was utilized.

Fusegi et al. (1992)investigated the effect of modifying the aspect ratio and Prandtl number in a differentially heated enclosure. The aspect ratio was changed between 0.3 and 5, with 5.85 being selected as the Prandtl number. When the aspect ratio was raised, a larger area of the heated wall was filled with downward flow, according to the findings. At greater aspect ratios, the heat flow along the outside hot wall was directed from the fluid to the environment throughout the majority of the height of the wall. Hdhiri et al. (2019) performed a numerical analysis of convection in a square cavity filled with porous media and internal heat generation for varied Grashoff numbers in the range of 10^3-10^6 and Prandtl numbers in the range of 0.015-0.054. The data demonstrated that increasing the Prandtl number had a considerable effect on average Nusselt number values, as well as relationships.

CHAPTER THREE: METHODOLOGY

In this chapter, the methodology that is applied for the work from the start of the project till the completion is described. The theoretical background of fluid flow inside a partitioned cavity and the computational details are also elaborated. A brief discussion of numerical methods available for solving a problem numerically is as well presented in this chapter. The methodology used during the thesis as shown are categorized into four stages as follows:

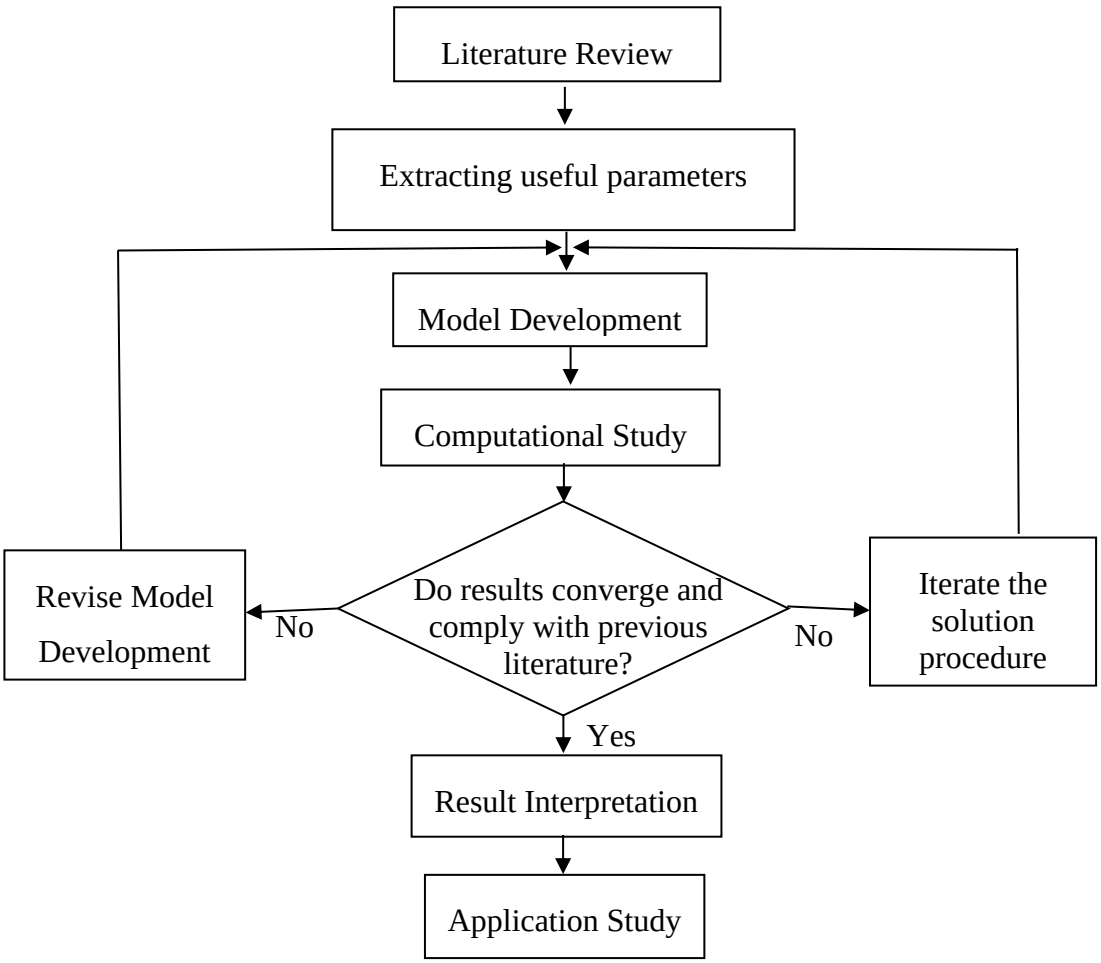

Figure 3.1 Flowchart depicting the research methodology adopted in this study.

3.1 First stage

3.1.1 Literature review

The review of previous literature encompasses the greater portion of the research methodology. Throughout the endeavor, books, journals, papers, and articles are fully examined and reviewed. Moreover, during the literature review research gaps and limitations has been identified and evaluated during this work.

3.2 Second stage

3.2.1 Model verification of previous work

The dimensions of the model to be constructed was obtained from a prior research publication in which a comparable geometry experiment was conducted. The developed model is used for numerical simulation by defining the suitable physics used and obtaining all the necessary boundary and initial conditions with the help of the same experimental research paper. The isotherm contour and streamline plots corresponding to the present study and H. Oztop & Bilgen, (2006) are compared to validate the present study.

3.3 Third stage

3.3.1 Computational study

Computation software is required to perform the calculations necessary for the simulation of fluid and surface interaction. Computational fluid dynamics is based upon Navier-Stokes equations which describes various interrelationship between properties of moving fluid. It has presently found its application in most of the processes requiring analysing of thermal properties and air flow modelling.

3.3.2 Application study

Among several applications, the study of double and triple paned glass windows is chosen for the application study field in which the comparative thermal and flow characteristics for the multiple paned windows is studied. Also, the numerical analysis is done to see the impact of changing *Ra* on the thermal and flow behavior inside the partitioned cavity.

3.4 Fourth stage

3.4.1 Documentation and presentation of the findings

The findings of the research work are presented in the form of conference article and formal thesis report according to the guidelines of Department of Mechanical and Aerospace Engineering, Pulchowk Campus, Institute of Engineering.

The methodology used for the study also includes defining the physical and mathematical model for the present study which are discussed in details as follow.

3.5 Physical problem

Two different cases of partition are discussed in this chapter. Governing equations, physical model and the boundary conditions for each case are presented in the following sections.

3.5.1 Wavy partition with single working fluid (air)

As shown in Figure 3.2, a two-dimensional enclosure of length L and height H is chosen, partitioned by a heat transmitting wavy solid wall of thickness $0.05L$ and thermal conductivity k_s, with differential heating and a uniform heat generating source in each domain. The enclosure's horizontal walls are adiabatic, while boundary vertical walls are kept constant at T_H and T_C, respectively. Air is the working fluid in each of the two fluid domains separated by the wavy barrier. Three alternative materials, namely plywood, glass fiber, and common brick, are evaluated in order to analyze the performance inside the partitioned cavity. Table 3.1 shows the corresponding thermal conductivity (k_s) of the partition materials as well as the thermal conductivity ratio (k_r) between solid partition and air.

3.5.2 Solid partition with two fluid zones

Figure 3.3 depicts an enclosure with side length L separated centrally by a heat transmitting vertical solid wall with thermal conductivity k_s. The horizontal walls of the enclosure are adiabatic, whereas the boundary vertical walls are maintained at T_C and T_H, respectively. The partition is kept at $x = c$ within the enclosure, splitting the enclosure into two convection domains filled with various types of working fluids and a conduction domain within the cavity's partition wall. In the left and right flow

domains, the working fluids are air and water, respectively. Common brick, plywood and glass fiber are chosen as the material of the partition in this present study.

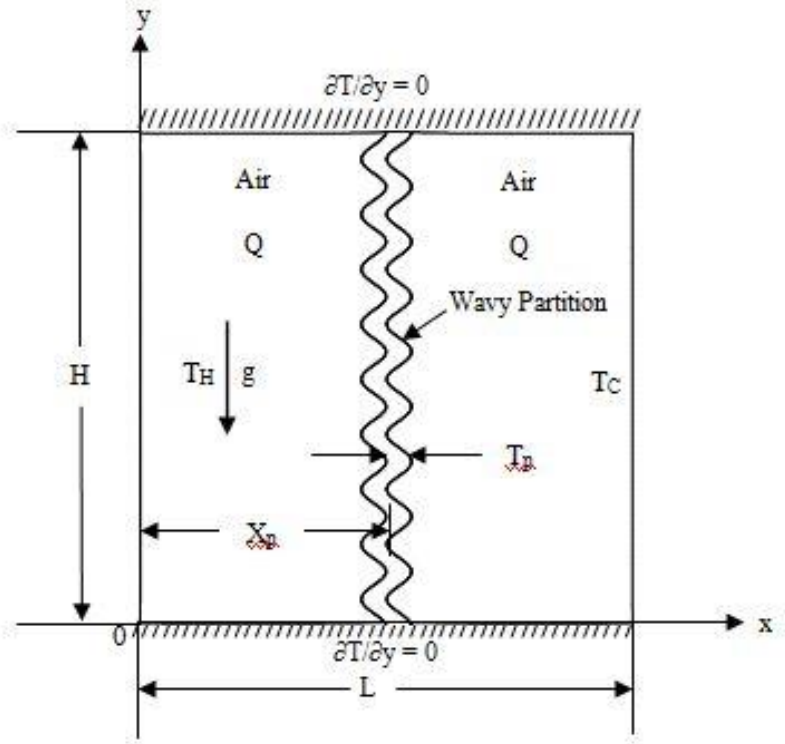

Figure 3.2 Diagram of enclosure with wavy partition along with boundary conditions.

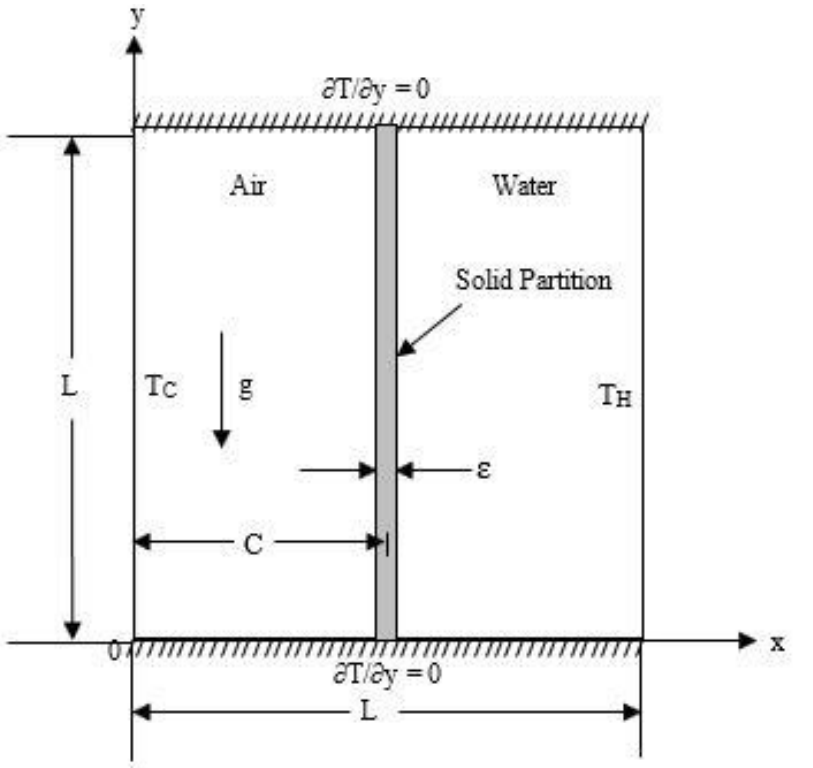

Figure 3.3 Diagram of enclosure with solid partition along with boundary conditions.

3.6 Governing equations

Formulations of governing equations for different cases in this thesis are discussed as follows:

3.6.1 Wavy partition with single working fluid

The thermophysical properties of air and water are considered to be constant. However, the change in density with the temperature of the working fluid in the body force is represented by Oberbeck-Boussinesq approximation. Using these considerations, the governing dimensional equations are given as follows:

$$\frac{\partial \vec{u}}{\partial x}+\frac{\partial \vec{v}}{\partial y}=0 \qquad \textit{Equation 3-1}$$

$$\rho_a\left(\vec{u}\frac{\partial \vec{u}}{\partial x}+\vec{v}\frac{\partial \vec{u}}{\partial y}\right)=-\frac{\partial p}{\partial x}+\mu_a\left(\frac{\partial^2 \vec{u}}{\partial x^2}+\frac{\partial^2 \vec{u}}{\partial y^2}\right) \qquad \textit{Equation 3-2}$$

$$\rho_a\left(\vec{u}\frac{\partial \vec{v}}{\partial x}+\vec{v}\frac{\partial \vec{v}}{\partial y}\right)=-\frac{\partial p}{\partial y}+\mu_a\left(\frac{\partial^2 \vec{v}}{\partial x^2}+\frac{\partial^2 \vec{v}}{\partial y^2}\right)+\rho_a g\beta\left(T-T_c\right) \qquad \textit{Equation 3-3}$$

$$\rho_a C_{p,a}\left(\vec{u}\frac{\partial T}{\partial x}+\vec{v}\frac{\partial T}{\partial y}\right)=k_a\left(\frac{\partial^2 T}{\partial x^2}+\frac{\partial^2 T}{\partial y^2}\right)+\vec{Q} \qquad \textit{Equation 3-4}$$

$$X=\frac{x}{L},Y=\frac{y}{L},\vec{U}=\frac{\vec{u}L}{\alpha_a},\vec{V}=\frac{\vec{v}L}{\alpha_a},P=\frac{pL^2}{\rho\alpha_a^2},\Theta=\frac{T-T_c}{T_h-T_c} \qquad \textit{Equation 3-5}$$

Considering the Oberbeck-Boussinesq approximation for buoyancy and assuming constant fluid properties, the dimensionless governing equations (*3-1*) - (*3-4*) in pressure-velocity formulation can then be written as follows:

$$\frac{\partial \vec{U}}{\partial X}+\frac{\partial \vec{V}}{\partial Y}=0 \qquad \textit{Equation 3-6}$$

$$\vec{U}\frac{\partial \vec{U}}{\partial X}+\vec{V}\frac{\partial \vec{U}}{\partial Y}=-\frac{\partial P}{\partial X}+\left(\frac{\partial^2 \vec{U}}{\partial X^2}+\frac{\partial^2 \vec{U}}{\partial Y^2}\right) \qquad \textit{Equation 3-7}$$

$$\vec{U}\frac{\partial \vec{V}}{\partial X}+\vec{V}\frac{\partial \vec{V}}{\partial Y}=-\frac{\partial P}{\partial Y}+\left(\frac{\partial^2 \vec{V}}{\partial X^2}+\frac{\partial^2 \vec{V}}{\partial Y^2}\right)+\frac{Ra_{ae}}{\mathrm{Pr}_a}\Theta \qquad \textit{Equation 3-8}$$

$$\vec{U}\frac{\partial \Theta}{\partial X}+\vec{V}\frac{\partial \Theta}{\partial Y}=\frac{1}{\mathrm{Pr}_a}\left(\frac{\partial^2 \Theta}{\partial X^2}+\frac{\partial^2 \Theta}{\partial Y^2}\right)+\frac{Ra_{ai}}{Ra_{ae}\,\mathrm{Pr}_a} \qquad \textit{Equation 3-9}$$

Where,

$$Ra_{ae}=\frac{g\beta\left(T_h-T_c\right)L^3}{\nu_a\alpha_a},\ Ra_{ai}=\frac{g\beta QL^5}{\nu_a\alpha_a k_a},\ Pr_a=\frac{\nu_a}{\alpha_a} \qquad \textit{Equation 3-10}$$

$$\frac{\partial^2 \Theta}{\partial X^2}+\frac{\partial^2 \Theta}{\partial Y^2}=0 \qquad \textit{Equation 3-11}$$

3.6.2 Enclosure with two fluid zones

The governing dimensional equations for the enclosure divided into two fluid zones are given as follows:

For air domain:

$$\frac{\partial \vec{u}}{\partial x}+\frac{\partial \vec{v}}{\partial y}=0 \qquad \textit{Equation 3-12}$$

$$\rho_a\left(\vec{u}\frac{\partial \vec{u}}{\partial x}+\vec{v}\frac{\partial \vec{u}}{\partial y}\right)=-\frac{\partial p}{\partial x}+\mu_a\left(\frac{\partial^2 \vec{u}}{\partial x^2}+\frac{\partial^2 \vec{u}}{\partial y^2}\right) \qquad \textit{Equation 3-13}$$

$$\rho_a\left(\vec{u}\frac{\partial \vec{v}}{\partial x}+\vec{v}\frac{\partial \vec{v}}{\partial y}\right)=-\frac{\partial p}{\partial y}+\mu_a\left(\frac{\partial^2 \vec{v}}{\partial x^2}+\frac{\partial^2 \vec{v}}{\partial y^2}\right)+\rho_a g\beta\left(T-T_c\right) \qquad \textit{Equation 3-14}$$

$$\rho_a C_{p,a}\left(\vec{u}\frac{\partial T}{\partial x}+\vec{v}\frac{\partial T}{\partial y}\right)=k_a\left(\frac{\partial^2 T}{\partial x^2}+\frac{\partial^2 T}{\partial y^2}\right) \qquad \textit{Equation 3-15}$$

For solid domain:

$$k_s\left(\frac{\partial^2 T}{\partial x^2}+\frac{\partial^2 T}{\partial y^2}\right)=0 \qquad \textit{Equation 3-16}$$

For water domain:

$$\frac{\partial \vec{u}}{\partial x}+\frac{\partial \vec{v}}{\partial y}=0 \qquad \textit{Equation 3-17}$$

$$\rho_w\left(\vec{u}\frac{\partial \vec{u}}{\partial x}+\vec{v}\frac{\partial \vec{u}}{\partial y}\right)=-\frac{\partial p}{\partial x}+\mu_w\left(\frac{\partial^2 \vec{u}}{\partial x^2}+\frac{\partial^2 \vec{u}}{\partial y^2}\right) \qquad \textit{Equation 3-18}$$

$$\rho_w\left(\vec{u}\frac{\partial \vec{v}}{\partial x}+\vec{v}\frac{\partial \vec{v}}{\partial y}\right)=-\frac{\partial p}{\partial y}+\mu_w\left(\frac{\partial^2 \vec{v}}{\partial x^2}+\frac{\partial^2 \vec{v}}{\partial y^2}\right)+\rho_w g\beta\left(T-T_c\right) \qquad \textit{Equation 3-19}$$

$$\rho_w C_{p,w}\left(\vec{u}\frac{\partial T}{\partial x}+\vec{v}\frac{\partial T}{\partial y}\right)=k_w\left(\frac{\partial^2 T}{\partial x^2}+\frac{\partial^2 T}{\partial y^2}\right) \qquad \textit{Equation 3-20}$$

$$X=\frac{x}{L},Y=\frac{y}{L},\vec{U}=\frac{\vec{u}L}{\alpha_a},\vec{V}=\frac{\vec{v}L}{\alpha_a},P=\frac{pL^2}{\rho\alpha_a^2},\Theta=\frac{T-T_c}{T_h-T_c},\alpha_a=\frac{k_a}{\rho_a c_{p,a}} \qquad \textit{Equation 3-21}$$

Using the above scales, the dimensional governing equations (*3-12*) – (*3-20*) can be transformed to a set of non-dimensional equations as follows:

For air domain:

$$\frac{\partial \vec{U}}{\partial X}+\frac{\partial \vec{V}}{\partial Y}=0 \qquad \textit{Equation 3-22}$$

$$\vec{U}\frac{\partial \vec{U}}{\partial X}+\vec{V}\frac{\partial \vec{U}}{\partial Y}=-\frac{\partial P}{\partial X}+Pr_a\left(\frac{\partial^2 \vec{U}}{\partial X^2}+\frac{\partial^2 \vec{U}}{\partial Y^2}\right) \qquad \textit{Equation 3-23}$$

$$\vec{U}\frac{\partial \vec{V}}{\partial X}+\vec{V}\frac{\partial \vec{V}}{\partial Y}=-\frac{\partial P}{\partial Y}+Pr_a\left(\frac{\partial^2 \vec{V}}{\partial X^2}+\frac{\partial^2 \vec{V}}{\partial Y^2}\right)+Ra_{ae}Pr_a\Theta \qquad \textit{Equation 3-24}$$

$$\vec{U}\frac{\partial \Theta}{\partial X}+\vec{V}\frac{\partial \Theta}{\partial Y}=\left(\frac{\partial^2 \Theta}{\partial X^2}+\frac{\partial^2 \Theta}{\partial Y^2}\right) \qquad \textit{Equation 3-25}$$

For solid domain:

$$k_r\left(\frac{\partial^2\Theta}{\partial X^2}+\frac{\partial^2\Theta}{\partial Y^2}\right)=0 \qquad \textit{Equation 3-26}$$

For water domain:

$$\frac{\partial\vec{U}}{\partial X}+\frac{\partial\vec{V}}{\partial Y}=0 \qquad \textit{Equation 3-27}$$

$$\frac{\rho_w}{\rho_a}\left(\vec{U}\frac{\partial\vec{U}}{\partial X}+\vec{V}\frac{\partial\vec{U}}{\partial Y}\right)=-\frac{\partial P}{\partial X}+\frac{\mu_w}{\mu_a}Pr_a\left(\frac{\partial^2\vec{U}}{\partial X^2}+\frac{\partial^2\vec{U}}{\partial Y^2}\right) \qquad \textit{Equation 3-28}$$

$$\frac{\rho_w}{\rho_a}\left(\vec{U}\frac{\partial\vec{U}}{\partial X}+\vec{V}\frac{\partial\vec{U}}{\partial Y}\right)=-\frac{\partial P}{\partial X}+\frac{\mu_w}{\mu_a}Pr_a\left(\frac{\partial^2\vec{U}}{\partial X^2}+\frac{\partial^2\vec{U}}{\partial Y^2}\right)+\frac{\rho_w}{\rho_a}Ra_{ae}Pr_a\Theta \qquad \textit{Equation 3-29}$$

$$\left(\vec{U}\frac{\partial\Theta}{\partial X}+\vec{V}\frac{\partial\Theta}{\partial Y}\right)=\frac{\alpha_w}{\alpha_a}\left(\frac{\partial^2\Theta}{\partial X^2}+\frac{\partial^2\Theta}{\partial Y^2}\right) \qquad \textit{Equation 3-30}$$

$$Ra_{ae}=\frac{g\beta(T_h-T_c)L^3}{\nu_a\alpha_a},Pr_a=\frac{c_{p,a}\mu_a}{k_a},Ra_w=\frac{g\beta(T_h-T_c)L^3}{\nu_w\alpha_w},Pr_w=\frac{c_{p,w}\mu_w}{k_w} \qquad \textit{Equation 3-31}$$

Table 3.1 List of various thermophysical properties of materials and fluid.

Proporties	Air	Water	Glass Fiber	Plywood	Common Brick
ρ (kg/m$^{3)}$	1.1275	991.80			
μ (Pa.s)	1.9148×10^{-5}	6.3544×10^{-4}			
k (W/m.K)	0.027076	0.63247	0.036	0.12	0.72
c_p (J/kg.K)	1006.9	4067.3			
α (m^2/s)	2.3848×10^{-5}	1.5679×10^{-7}			

3.7 Boundary conditions

Table 3.2 Boundary conditions corresponding to the present study

Dependent variables	Left wall	Right wall	Top and bottom walls	Partition walls	
				Left side	Right side
Velocity	$U = V = 0$	$U = V = 0$	$U = V = 0$	$U = V = 0$	$U = V = 0$
Temperature	$\Theta = 1$	$\Theta = 0$	$\frac{\partial \Theta}{\partial Y} = 0$	$\frac{k_s}{k_a}\frac{\partial \Theta}{\partial X}\Big\|_s = \frac{\partial \Theta}{\partial X}\Big\|_a$	$\frac{k_s}{k_a}\frac{\partial \Theta}{\partial X}\Big\|_s = \frac{\partial \Theta}{\partial X}\Big\|_a$

3.8 Performance parameters

The mean dimensionless parameters governing the performance of this problem are *Nu* and Θ_{av} which are presented as follows:

3.8.1 Average Nusselt number

$$Nu_H = \int_0^1 \left(\frac{\partial \Theta}{\partial X} \right)_{X=1} dy \qquad \textit{Equation 3-32}$$

$$Nu_C = \int_0^1 \left(\frac{\partial \Theta}{\partial X} \right)_{X=0} dy \qquad \textit{Equation 3-33}$$

3.8.2 Average bulk temperature

It is the ratio of sum of temperatures of the fluid inside the cavity at various locations to area of the cavity. It reflects the mean temperature at different locations inside the cavity and denotes the behavior of temperature gradient inside the enclosure. It is represented as follows:

$$\Theta_{av} = \frac{1}{A_f} \int_{A_f} \Theta_f \, dA_f . \qquad \textit{Equation 3-34}$$

CHAPTER FOUR: RESULTS AND DISCUSSION

4.1 Thermal performance in an enclosure with two fluid zones

Different values of thickness ($0.05L \leq \varepsilon \leq 0.2L$), location ($0.25L \leq c \leq 0.75L$) and three different materials (glass fiber, plywood and common brick) of the partition are selected to carry out the investigation. Besides, varying Ra_a is also selected ranging from $Ra_a = 10^3 - 10^6$ ($Ra_w = 4.032\times10^6 - 4.032\times10^9$). Hence, the effects of thickness, position and material of the partition on the thermal and flow performance inside the differentially heated enclosure is analyzed. Three different values of $k_r = k_s/k_a$ = 1.39, 4.63 and 27.8 corresponding to glass fiber, plywood and common brick respectively are considered for the non-dimensional numerical simulations.

4.1.1 Impact of variation of thickness of partiton

Streamlines and isothermal contours resulting from the numerical simulations for constant $c = 0.50L$ and k_s = 0.12 W/m.K for different thickness of the partition corresponding to $Ra_a = 10^3$ and 10^6 are presented in Figures A1 and A2 respectively to study the thermal and flow performance in the cavity. The thermal exchanges from the hot wall across the water regime passing though the partition wall to the air regime towards the cold wall is observed to be mostly confined in the left domain. The variation of temperature across the hot wall and the partition enclosing water filled chest is negligible which is evident from the isothermal contours as shown in Figure A1. It is obvious from the isotherm plots that the left convective region is conduction dominant owing to smaller Ra_a. As the Rayleigh number in the right convective region is much higher than that of the left one, the isotherm lines are distorted in the water filled convective region. However, most of the thermal exchange occurs into left convective region due to the higher temperature difference and the otherwise is visible in the right convective region. At low Rayleigh number, convective area in the left domain decreases increasing the heat flow due to the dominance of conduction. At higher Rayleigh number, the isotherm plot in the left domain becomes distorted. Moreover, in the right domain greater distortion of the isotherm plots are observed. The thickness of the boundary layer decreases with the rise in the distortion of the isothermal plots which is seen from Figure A1.

Figure A2 shows the flow patterns corresponding to various partition wall thickness and its variation with the increase in Ra_a. At low Ra_a, the streamline plots are counter clockwise in direction and oval shaped in each of the both air and water convective region. However, the strengths of the flow fields are comparatively stronger in the air-filled convective region compared to that of the water filled convective region. Similarly, with rise in partition thickness, flow field strength in each convective region decreases as convection area declines across which fluid flows. As Rayleigh number increases to a higher value, the oval shaped streamlines are transformed into elongated distorted shapes. However, the degree of distortion is observed to be lower in the air convective region than the water convective region. The streamlines are found to be almost flat and parallel with horizontal walls in the central region of the water filled domain with the clustering of streamlines along the side and partition walls. Similarly, a distinct layer of boundary layer is formed in the water filled convective region. The strength of the flow fields is greatly enhanced in the left region at high Ra_a due to the dominance of convection. In contrast, as partition thickness rises and convection dominance, the convection currents strength remains almost the same.

The fluid temperatures are plotted in Figure 4.1 to show the change in temperature due to varying thickness of the partition. As the Rayleigh number increases in the air convective region, convective currents are increased causing better thermal exchange across the air-filled region. Hence, with an increase in the Ra_a, average fluid temperature in the air convective region decreases. Similarly, in the water convective region, with an increase in Ra_w, insignificant change in the convective currents are seen which results in almost constant thermal exchange rate and almost constant $\Theta_{av,w}$ in the water filled convective region. Moreover, with rise in partition thickness, area through which the thermal exchange occurs decreases resulting in a higher thermal exchange rate across the fluid regions. Thus, the thermal exchange rate corresponding to a high thickness partition is greater resulting in lower average fluid temperature compared to that of the low thickness partition.

The comparison in the Nusselt number dictates that the values of Nu along the hot wall are significantly lower compared to that along the clod wall. This is due to the difference in the buoyancy force between the two fluids contained in the two convective regions. As the buoyancy force in the right cavity near the hot wall is higher due to the higher

density of water than air, the convective currents are low in the right convective region. As a consequence, less thermal exchange rate is observed in the right cavity compared to that of the left cavity. It is obvious from Figure 4.2 that, for low *Ra* the cavity is conduction dominant, however with the increase in Ra_a ($Ra_a \geq 10^4$), convection becomes dominant inside the cavity causing improved thermal exchange in each domain. In case of partition thickness, at low Ra_a ($Ra_a \leq 10^4$), partition of higher thickness shows higher thermal exchange rate than lower thickness of the partition. This is due to the increasing heat conducting area of the partition for increasing thickness, which induces higher conduction thermal exchange for conduction dominant low Ra_a. However, when the cavity is convection dominant, partition of higher thickness results in small convection regions and larger conducting area, which results in low thermal exchange as the partition opposes the heat flow through it.

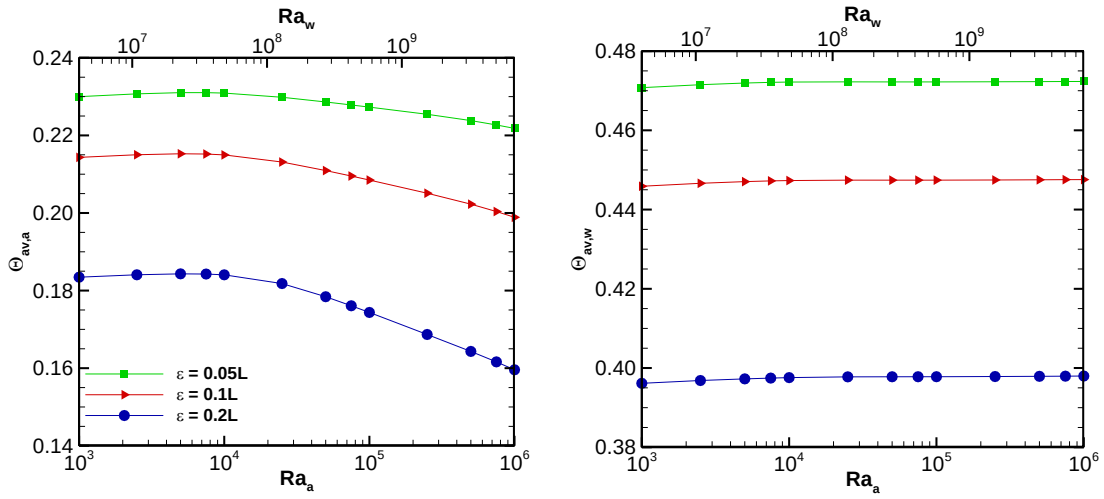

(a) (b)

Figure 4.1 Change in fluid temperature for various thickness and Rayleigh numbers at $c = 0.50L$ and $k_s = 0.12$ W/m.K.

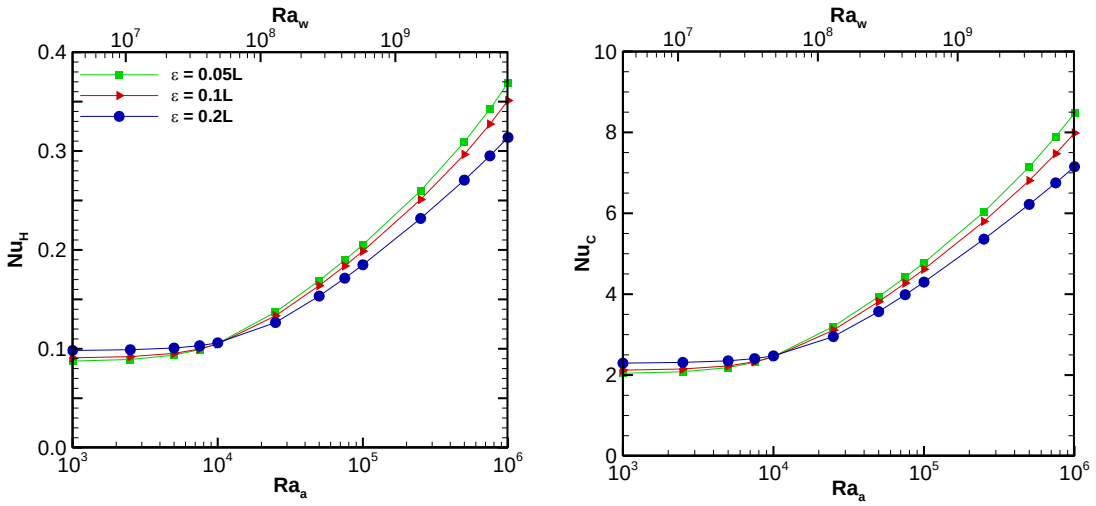

(a) (b)

Figure 4.2 Change in Nusselt number for various thickness and Rayleigh numbers at $c = 0.50L$ and $k_s = 0.12$ W/m.K.

4.1.2 Impact of variation of position of partition

Numerical simulation were carried out for constant $k_s = 0.72$ W/m.K and $\varepsilon = 0.1L$ to study the effects of variation of position of the partition inside the cavity. Figures A3 and A4 shows isotherm plots and streamlines respectively for $Ra_a = 10^3$ and 10^6 which are studied to evaluate the thermal and flow performance inside the cavity across air and water regions. It is also observed that the thermal exchange rate is accelerated in the air region and the thermal exchange rate is accompanied by conduction at low Rayleigh number as seen from Figure A3. Moreover, with the increase in distance of the partition from the cold wall, the area of the air convective region increases and the distribution of the isotherm plots are spread out across the region. In the similar manner, the convective are in the water region is reduced and thus the isotherm plots are confined in a smaller area. The dominance of convection is observed and thus the isotherm plots are further distorted in both convective regions.

It is seen that, at low Ra_a, the streamlines are as well counterclockwise in direction and almost oval shaped in each of the convective regions. However, the strength of the flow fields is comparatively lower than those compared to rest of the cases in the present study. Moreover, the strength of the flow fields in the air region is lower in comparison to the water region when the partition wall is closest to left wall. A considerable change in the flow field strength is seen with the increase in the position of the partition owing to the greater conducting are in the air region, which allows the smooth flow of fluids.

Moreover, when *Ra* is increased, distortion of the flow fields is observed in both the convective regions. As convection is more dominant at higher *Ra*, thermal and flow performance are enhanced with the increasing Ra_a. The hydrodynamic boundary layers are evidently formed in the water domain. As seen from Figure A4. The streamlines are confined to a smaller are in the water convective region with an increase in the position of the partition. However, greater convective area is available for the thermal exchange in the air convective region, thereby increasing the flow field strength.

Moreover, in the air convective region, when the position from cold wall increases, greater thermal exchange area is observed and better thermal performance is observed and the thermal exchange rate across the air medium is reduced, which eventually rises the average fluid temperature in the convective region. The closer the partition is placed to the cold wall, greater thermal exchange is observed resulting in lower $\Theta_{av,a}$. In contrast, in the water convective region, the closer the partition is to the hot wall, greater thermal exchange rate is observed which results in lower average fluid temperature for the farthest position of the partition from the cold wall. The average fluid temperature in the water region is found to maximum as the dividing partition is positioned near cold wall, allowing the heat to accumulate and increasing the average fluid temperature. This value of $\Theta_{av,w}$ is found to be the highest compared to other cases considered in this present study.

At lower Ra_a, the average Nusselt number corresponding to $c = 0.25L$ is significantly larger compared to other positions due to the variation of thermal conductivities of fluids in the chests. As Ra_a increases, average Nusselt number becomes nearly equal and the variation is negligible.

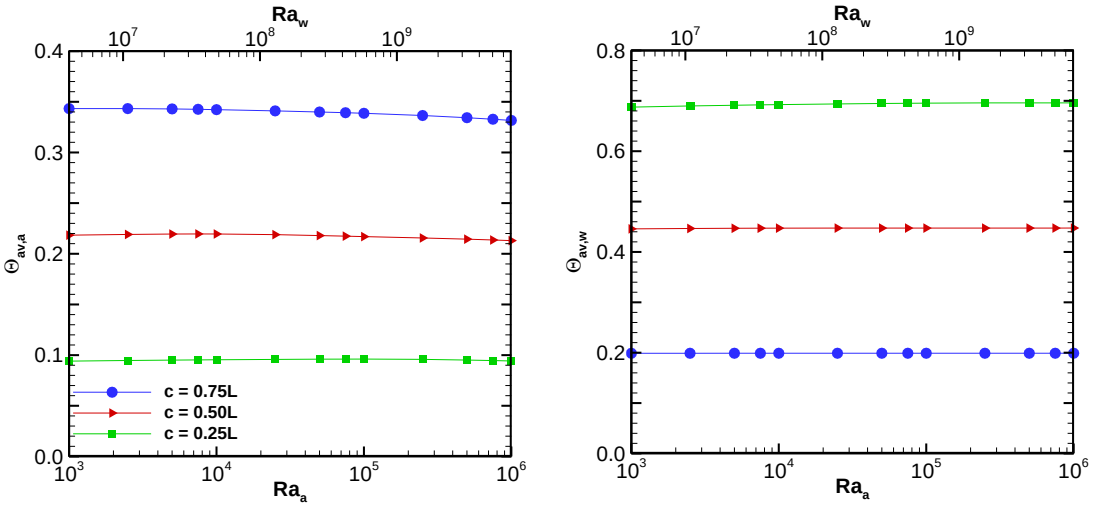

(a) (b)

Figure 4.3 Change in fluid temperature for various positions and Rayleigh numbers at $\varepsilon = 0.1L$ and $k_s = 0.72$ W/m.K.

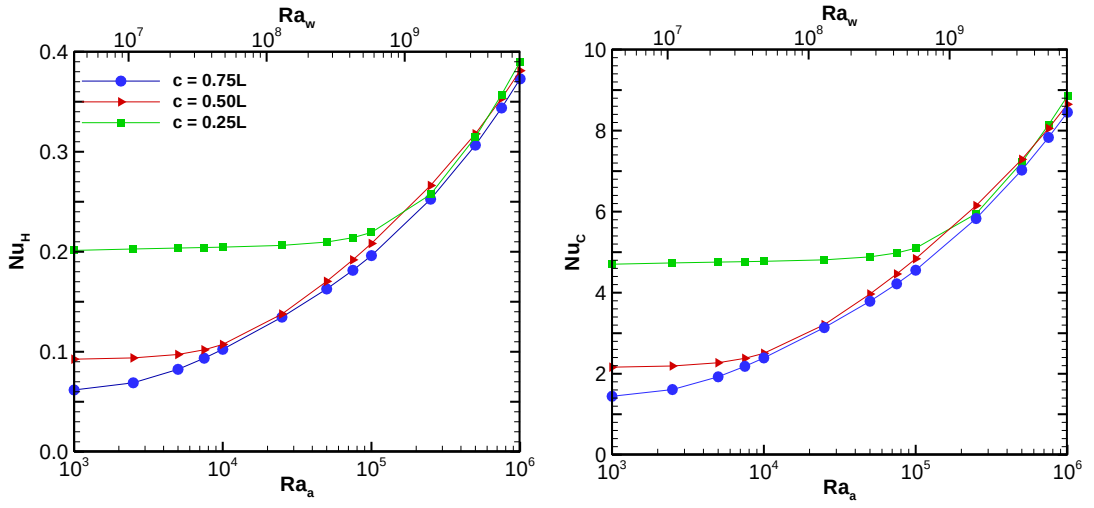

(a) (b)

Figure 4.4 Change in Nusselt number for various positions and Rayleigh numbers at $\varepsilon = 0.1L$ and $k_s = 0.72$ W/m.K..

4.1.3 Impact of variation of material of partition

Figures A5 and A6 displays the temperature profiles and streamlines respectively to observe the effect of different material of the partition the simulations have been carried out for $\varepsilon = 0.1L$ and $c = 0.50L$ and a wide range of Ra_a ($10^3 \leq Ra_a \leq 10^6$) varying the material of the partition. Here, the isotherms and the streamlines are also distorting with

increase in Ra_a. For low Ra_a the isotherms are almost evenly distributed horizontally throughout the whole cavity. The temperature profiles are accumulated near the sidewalls and the partition walls indicating the higher thermal exchange along the vertical wall. Similarly, Figure A6 presents the variation of streamlines with the Ra_a for different values of thermal conductivity of the material of the partition. Initially, the velocity profiles were egg shaped with lower strength. However, with the increase in Ra_a, the streamlines began to elongate and acquire greater strengths of fluid flow, thereby escalating the thermal performance. However, with increasing the thermal conductivity there seem to be almost no change in the streamlines.

With the increase in Ra_a the air convection region becomes convection dominant. Due to low k_r, less heat is transferring through it across the water convective region whereas more thermal exchange is taking place owing to the dominance of buoyancy driven heat flow in the air domain which in turns lowers the average temperature in the air domain.

It is evident from the figures that the thermal exchange increases with the increase in the thermal conductivity of the material of the partition. Moreover, the thermal exchange increases significantly with the increase in Ra_a.

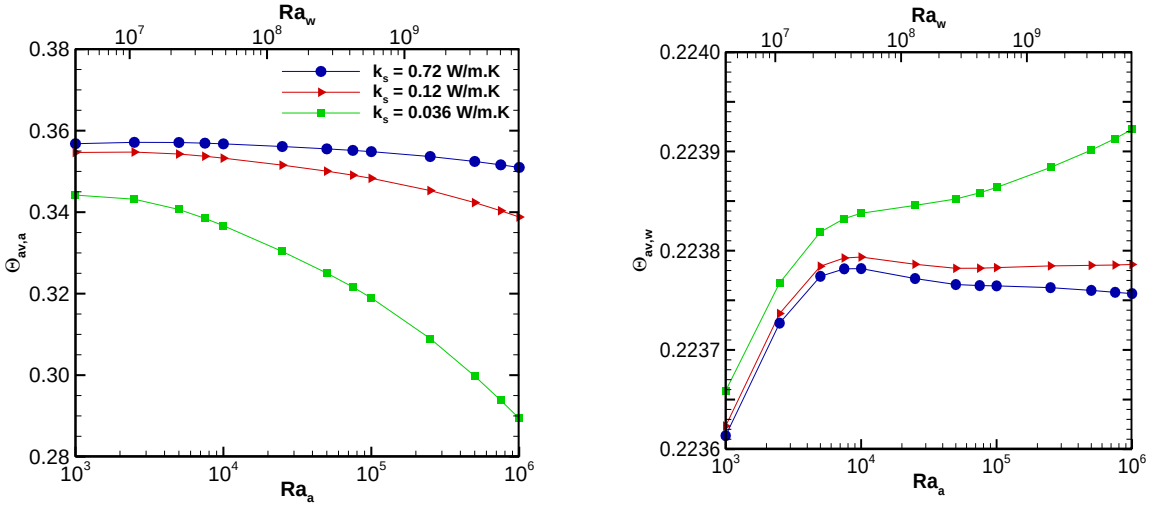

(a) (b)

Figure 4.5 Change in fluid temperature for various materials and Rayleigh numbers at $\varepsilon = 0.1L$ and $c = 0.50L$.

The thermal exchange in the water domain is entirely due to conduction owing to the minimum fluid motion in the water filled cavity. On the other hand, thermal exchange

is mostly a result of convection in the air-filled cavity due to the higher strength of fluid motion inside the air-filled cavity.

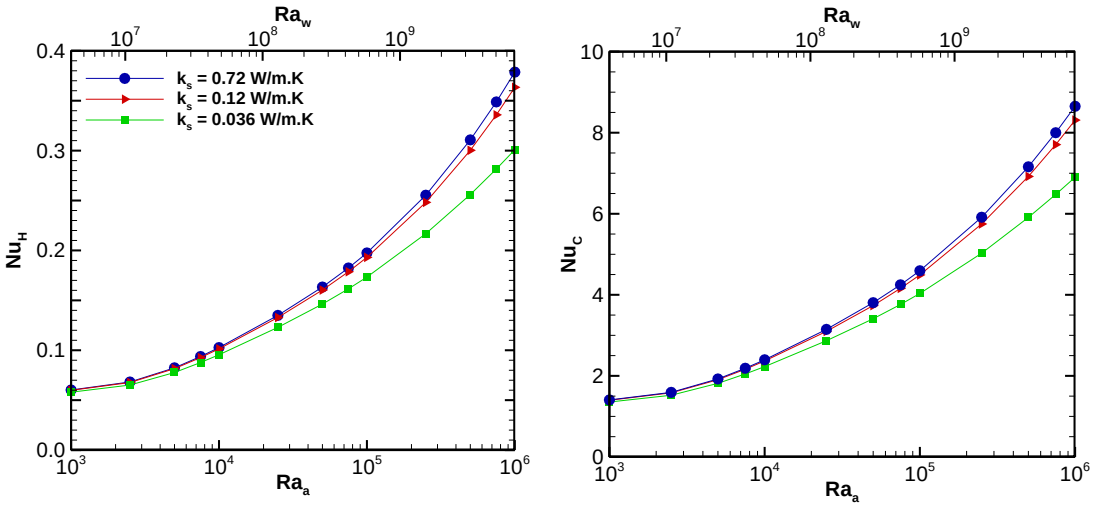

(a) (b)

Figure 4.6 Change in Nusselt number for various materials and Rayleigh numbers at $\varepsilon = 0.1L$ and $c = 0.50L$.

4.2 Thermal performance in an enclosure with wavy partition

Investigations are performed for different values of position (X_p = 0.25L, 0.50L and 0.75L), frequencies (f = 6, 9 and 12) and materials (k_r = 1.39, 4.63 and 27.8) of the wavy partition inside an enclosure. The computations were carried out over varying external Ra ($Ra_{ae} = 10^3 \sim 10^8$) and for constant internal Rayleigh number ($Ra_{ai} = 10^3$). For these numerical models, the working fluid was taken to be air (Pr_a = 0.71) while the thickness of the partition was kept constant at T_p = 0.05L.

4.2.1 Impact of variation of position of partition

The impact of location of partition on thermal and flow performance inside the enclosure is observed by means of performing numerical simulations for X_p = 0.25L, 0.50L and 0.75L at constant f = 9 and k_r = 1.39 and for a varying external Ra($10^3 \leq Ra_{ae} \leq 10^8$).

Contour plots for X_p = 0.25L, 0.50L and 0.75L corresponding to $Ra_{ae} = 10^4$ and 10^8 are chosen here to analyze the general characteristics. As mentioned earlier, the heat conducting wavy partition wall separates the enclosure into two separate convection regions.

The effect of the position of the wavy partition of the wavy partition from the left wall on the flow field is analyzed for $Ra_{ae} = 10^4$ and 10^8 and different position of the partition $X_p = 0.25L$, $0.50L$ and $0.75L$ as shown in Figure B2. When the *Ra* is low ($Ra_{ae} = 10^4$), lower convection currents are observed. Moreover, the rotating vortices in each fluid domain are clockwise in direction. The surface waviness imparts a distorted shape to the streamline along the partition. Streamline plots of Figure B2 indicates no significant variation in the flow field as the position of the wavy partition increases from the left wall. The oval shaped streamlines transform into straight lines that are somewhat parallel to each other and the streamlines vary in the core area as the external *Ra* increases. Similarly, the streamline near the wavy partition attains the shape of the wavy partition. Moreover, the position of the partition also has an insignificant impact on the shape of the flow field along the wavy partition walls. It is also observed that, with the increase in position from the hot wall, the streamline becomes more distorted and clustered in the vicinity of the wavy partition.

For higher as well as lower Ra_{ae}, the thermal exchange performance for the various positions of the wavy partition is comparable to each other while the thermal exchange performance improves with the increase in values of external *Ra*. The variation in the Nusselt number shows increase in the thermal performance with the increase in Ra_{ae}. However, with the increase in the location of the partition from the hot wall, no significant variation in the thermal exchange is observed which can be attributed to the internal heat generation in each of the domains.

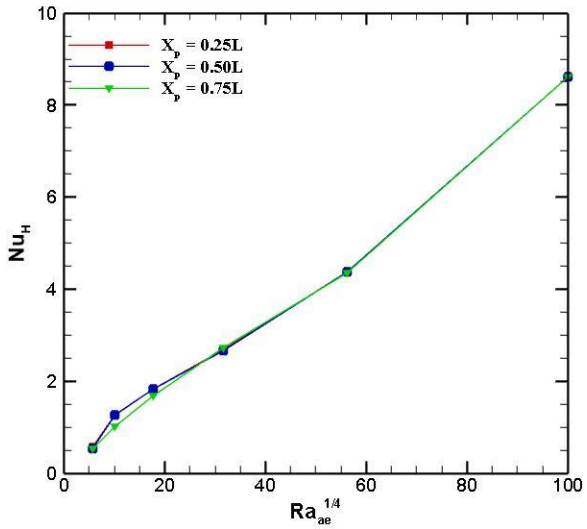

Figure 4.7 Change in Nusselt number for various positions at $f = 9$ and $k_r = 1.39$.

The heat generated causes the thermal exchange to be increasing at a rate comparable to each location. Similarly, the fluid temperature in each domain is observed to a decreasing function of Ra_{ae}. The fluid temperature corresponding to the position closest to hot wall is observed to the greatest and declines with the increase in location.

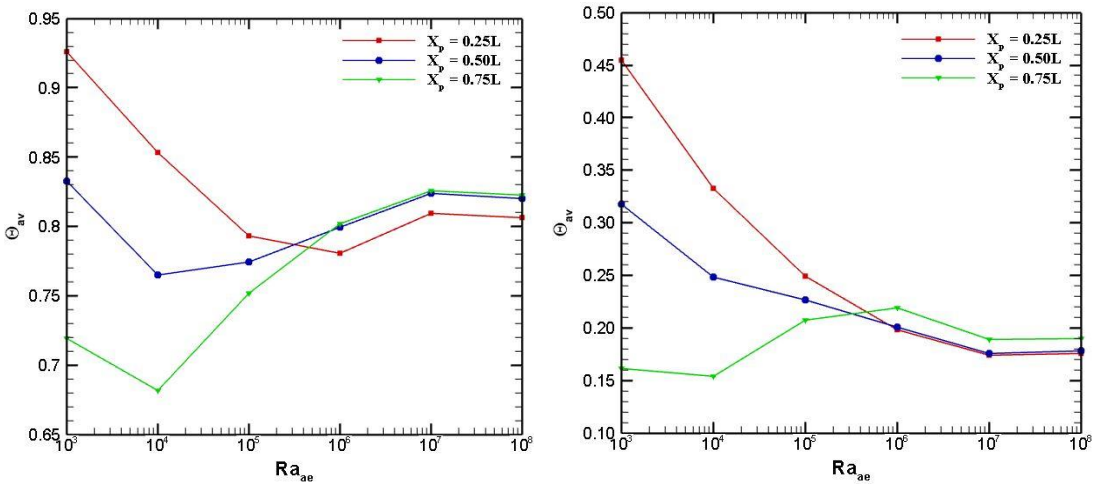

Figure 4.8 Change in fluid temperature for various positions at $f = 9$ and $k_r = 1.39$.

4.2.2 Impact of variation of frequency of partition

Numerical simulations have been carried out for frequencies, $f = 6$, 9 and 12 for varying external *Ra* ($10^3 \leq Ra_{ae} \leq 10^8$) to analyze the impact of different waviness frequencies on the thermal and flow behavior in an enclosure of $a_r = 2$. The position of the partition ($X_p = 0.50$), thermal conductivity ratio ($k_r = 4.63$) and internal Ra ($Ra_{ai} = 10^3$) has been kept constant for the present study. Isotherm plots, streamline plots, average bulk and Nusselt number are used to present the result of the numerical simulation.

Figure B3 visualizes the effect of variation of frequency of the waviness of the partition and external *Ra* on the thermal field inside an enclosure of $a_r = 2$. In order to understand the general characteristics, isotherm contours corresponding to $f = 6$, 9 and 12 and $Ra_{ae} = 10^4$ and 10^8 are chosen for representation. The wavy partition separates the enclosure into two separate regions. It is also observed that the two separate fluid domains are each in different thermal states, owing to the variation of the thermal boundary conditions on the differentially heated side walls, as seen from Figure B3. At low external *Ra* ($Ra_{ae} = 10^4$), the convection current is relatively low causing thick thermal boundary layer to develop at the wavy partition. It is seen from Figure B3 that,

insignificant change in the thermal field is observed with an increase in waviness frequency maintained at low external *Ra*. The effect is more pronounced at higher *Ra*, where the impact of the variation of the frequency of the waviness of the partition on the thermal boundary layer development is easily distinguishable. As Ra_{ae} increases, the isotherm plots distortion begins and the temperature contour lines becomes moreover parallel to each other. Increase in the frequency of the waviness of the partition implies a change in the physical geometry of the partition wall, which, in turn distorts the isotherm contour lines in the neighborhood of the partition wall. This implies, greater the frequency of the waviness, greater is the distortion of the isotherm plots near the walls, and thus convection currents are also amplified in these regions. Similarly, for low Ra_{ae}, the wavy partition hinders the thermal exchange thermal exchange owing to the less prominent conduction in this region. The conduction heat flow is more enhanced with the increase in Ra_{ae}, since the temperature difference now is greater and therefore the temperature contour plots are more distorted in the vicinity of the wavy partition solid wall.

Similarly, in order to analyze the effect of variation of frequency of the waviness of the partition and external Ra on the flow pattern in the differentially heated enclosure of $a_r = 2$, visualization of streamline for $f = 6$, 9 and 12 and $Ra_{ae} = 10^4$ and 10^8 is done as shown in Figure B4. At low external Ra ($Ra_{ae} = 10^4$), as mentioned earlier, the convective currents are comparatively low and the streamlines formed in each separated fluid domains are oval in shape and rotating clockwise in direction. The geometry of the wavy partition imparts slight distortion of the streamline in interaction with the surface of each side of the wavy partition wall. The change of frequency has no appreciable deviation of the streamline at low Ra_{ae} as seen from streamline plots corresponding to $Ra_{ae} = 10^4$ at varying frequency of the waviness of the partition wall as seen from Figure B4. However, at high external Ra ($Ra_{ae} = 10^8$), distortion of the streamline starts at the central region of each convective domain. The oval shaped streamline plots at lower Ra_{ae} changes to straight and almost parallel streamlines which are parallel to each other at high Ra_{ae}. As the frequency of the waviness increases, so does the distortion of the streamline in interaction with the wavy surface of the partition wall.

The variation of *Nu* with increasing Ra_{ae} for varying frequency is presented in Figure 4.9. The graph indicates that, the average *Nu* is distinctly differed for increasing value of frequencies of waviness of the partition in the square cavity.

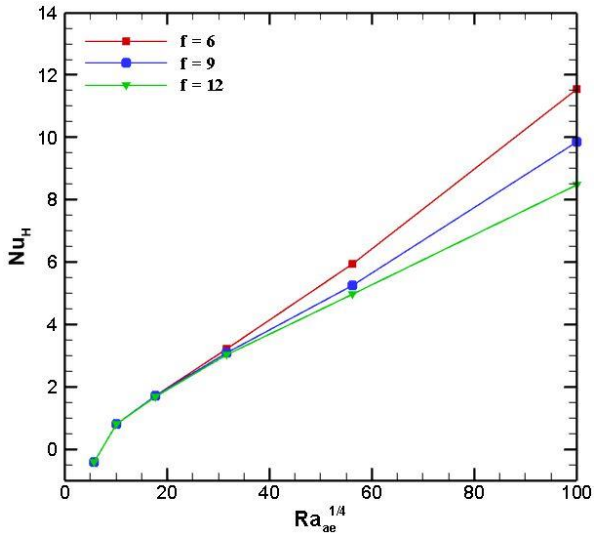

Figure 4.9 Change in Nusselt number for various frequency at $X_P = 0.5L$ and $k_r = 4.63$.

The fluid temperature in the left domain decreases and assumes the similar values for lower values of Ra_{ae}. However, at higher Ra_{ae}, the value increases slightly and is greatest for the greater frequency. Similarly, in the right domain, the average temperature corresponding to $f = 12$ shows contrasting values compared to other values of frequency.

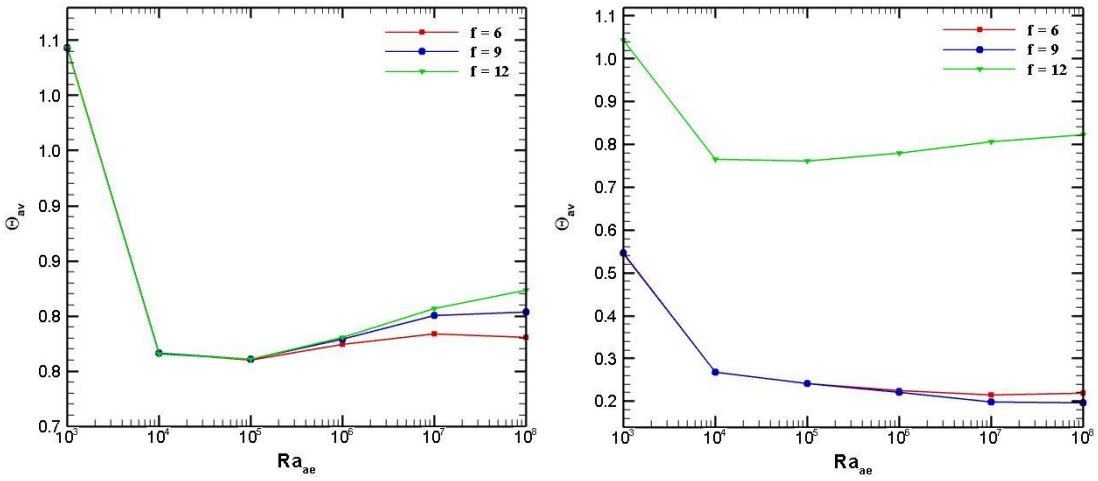

(a) (b)

Figure 4.10 Change in fluid temperature for various frequencies at $X_P = 0.5L$ and $k_r = 4.63$.

4.2.3 Impact of variation of material of partition

Similarly, to evaluate the impact of variation of changing material of the wavy partition and external *Ra* on the thermal exchange and flow characteristics inside an enclosure of aspect ratio (a_r = 0.5), numerical simulations for k_r = 1.39, 4.63 and 27.8 for varying external *Ra* ($10^3 \leq Ra_{ae} \leq 10^8$) for constant X_p = 0.25 and f = 12, were performed.

As the k_r of the material increases, no major changes in the temperature field are obtained for low values of Ra_{ae}. However, significant variation in the boundary layer is obtained as the external Ra increases. Distortion of the isotherm plots is observed and each fluid domain fills with almost straight and parallel temperature contours. There is no mentionable influence of the varying k_r on the thermal field at higher values of Ra_{ae} as well. The distortion of the thermal field near the partition walls can be attributed to greater convection currents in the vicinity of the partition walls.

Figure B6 visualizes the impact of variation of different material of the wavy partition and the external *Ra* on the flow field inside the differentially heated partitioned enclosure in terms of streamlines plots for $Ra_{ae} = 10^4$ and 10^8 corresponding to different thermal conductivity ratios (k_r = 1.39, 4.63 and 27.8). At low Ra ($Ra_{ae} = 10^4$), the convection currents are low and the streamline patterns are oval shaped. The vortices developed are rotating in clockwise direction in each of the two separated fluid domains. The streamlines in the vicinity of the partition wall takes the distorted shape of the geometry of the wavy partition wall. There is no prominent variation in the streamline pattern as the values of k_r are increased which is seen from Figure B6. As the value of Ra_{ae} increases, the streamlines begin to distort and become straight line. The streamlines thus, formed in the central core region in each fluid domain is almost parallel with each other, which is visible from Figure B6. The constant geometry of the partition wall imparts the distorted shape to the streamlines near the partition walls. At higher values of Ra_{ae}, with the increase in the value of k_r, no significant variation on the flow field is obtained and similar streamline strength for different k_r is also clearly evident from Figure B6.

Also, the fluid temperature between domains of cavity is presented in Figure 4.12 to show the change in temperature due to partition. The average temperature in both the domains shows a decreasing behavior at lower values of Ra_{ae}. In the left domain, the

average temperature value corresponding to lower thermal conductivity ratio has the greater value which is opposite in the case of right domain.

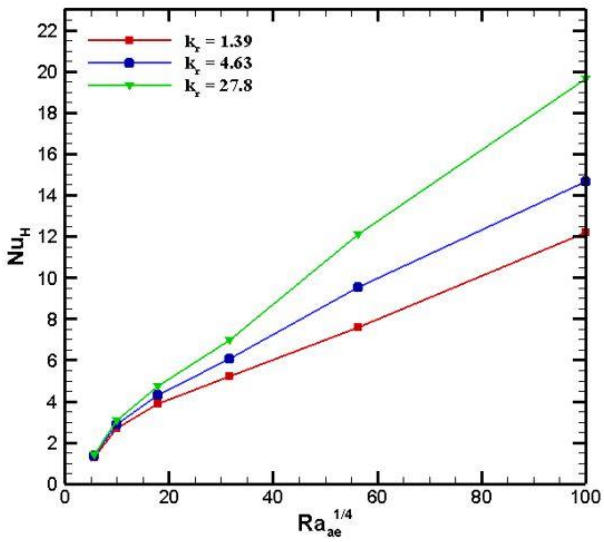

Figure 4.11 Change in Nusselt number for various materials at $X_p = 0.25L$ and $f = 12$.

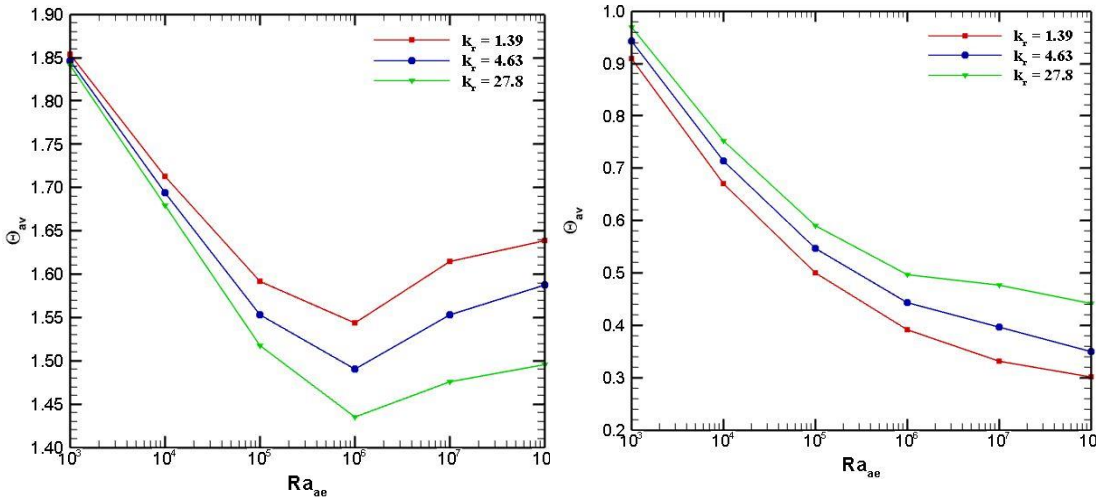

(a) (b)

Figure 4.12 Change in fluid temperature for various materials at $X_P = 0.25L$ and $f = 12$.

4.3 Comparative analysis

The thermal flow performance in an enclosure with air as the working fluid has been analyzed in this study. The cavity with and without any internal heat generation and divided by a solid and wavy partition were studied. The *Nu* variation with the *Ra* for both the cases are compared to evaluate thermal performance inside an enclosure.

4.3.1 Solid vs. wavy partitioned cavity without any internal heat generation

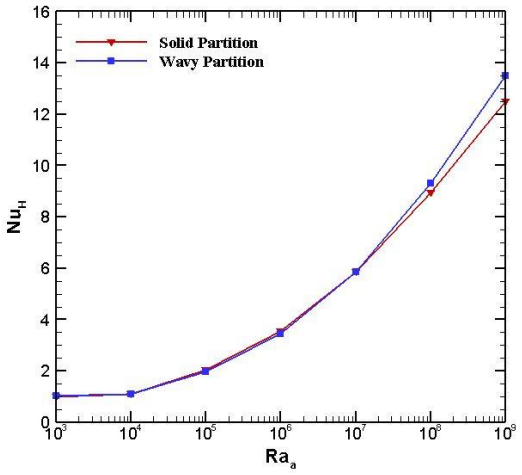

Figure 4.13 Change of Nusselt number with Rayleigh number for a cavity without any internal heat generation.

Numerical simulations corresponding to k_r= 27.8 and centrally placed solid and wavy partition in an enclosure with air as the working fluid and without any internal heat generation is performed to evaluate variation in thermal exchange performance. No significant variation between the solid and wavy partitioned cavity is observed at lower values of Ra as seen from Figure 4.13. The Nusselt number corresponding to lower values of Ra are comparable for both the solid and wavy partition owing to the laminar flow of fluid and heat inside the cavity causing negligible change in its value. However, as the flow progresses to turbulent flow at higher Ra, certain variation is observed in the values of the Nusselt number. The *Nu* corresponding to $Ra_{ae} = 10^9$ suggests a variation of around 8% among the solid and wavy partition depicting that the thermal performance improves with the use of wavy partition instead of solid partition at higher values of Ra.

4.3.2 Solid vs. wavy partitioned cavity with internal heat generation

Similarly, numerical simulations corresponding to k_r = 27.8 and centrally placed solid and wavy partition in an enclosure with air as the working fluid and filled with heat generating fluid assessed to evaluate the variation in thermal exchange performance inside an enclosure. The variation in the *Nu* at lower *Ra* shows better thermal performance corresponding to the solid partition owing to the separation zones formed

near the wavy walls that eventually reduces thermal flow across the partition as depicted in Figure 4.14.

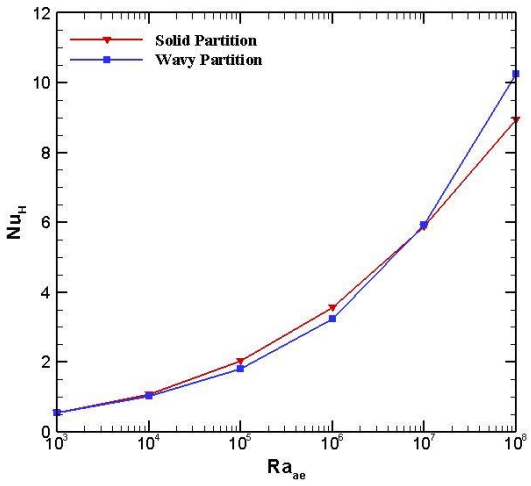

Figure 4.14 Change of Nusselt number with Rayleigh number for a cavity with internal heat generation.

However, as the flow progresses to turbulent flow at higher Ra, significant variation is observed in the values of the *Nu*. In a cavity filled with heat generating fluid, the Nusselt number corresponding to $Ra_{ae} = 10^8$ indicates a change of around 15% between the solid and wavy partition, indicating that the thermal exchange performance improves when the wavy partition is used instead of the solid partition at higher Ras. The heat generating fluid inside an enclosure enhances the thermal exchange performance to some extent as compared to the cavity without any internal heat generation as observed in this study

4.4 Application study

Researchers of thermal exchange are constantly looking for new ways to improve thermal exchange performance through various methods of thermal exchange enhancement. In an attempt to analyze the behavior of thermal exchange in glass pane windows, an application study of the current model is used to assess the thermal performance in double and triple pane window.

Similarly, for the triple pane window, an additional glass pane of the same thermal conductivity ratio is placed midway between the two glass panes at a distance of $X_P/2$ from each of the glass pane as shown in the figure below. The left and right glass panes are kept at a constant temperature and radiation effects across the two boundary glass panes are assumed to be negligible in this study

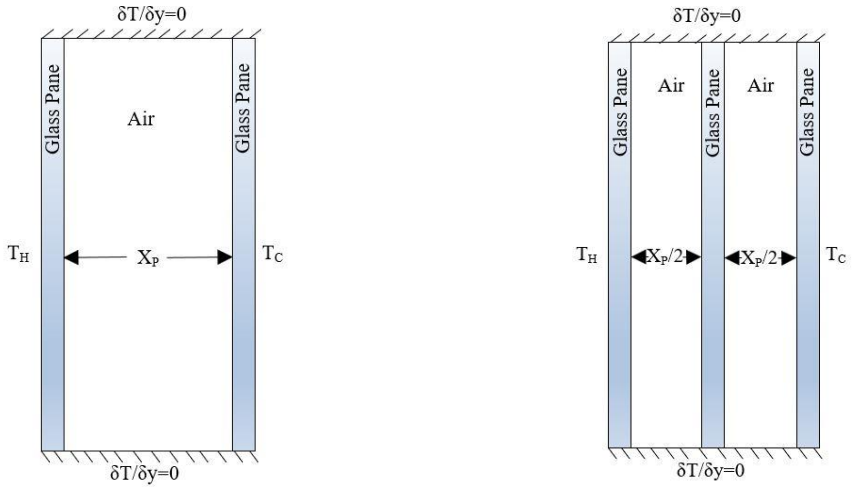

Figure 4.15 Diagram showing the physical modelling of double and triple pane window.

It is already established that the introduction of partition inside an enclosure reduces the thermal exchange and the effects of change of various physical parameter of the partition is also analyzed in this study. Similarly, as evident from Figure 4.16, the thermal exchange performance is greatly influenced with the introduction of an additional glass pane. The change in the *Nu* with the *Ra* for the double and triple pane window also suggests that the extra glass pane further restricts the fluid flow and thermal exchange. Results show that the thermal exchange performance of the triple pane window reduced by more than 50% as compared to the double pane window over varying *Ra*. The air gap formed in between the glass pane and the extra glass pane in between further restricts the thermal exchange and thus a significant reduction in thermal performance can be seen.

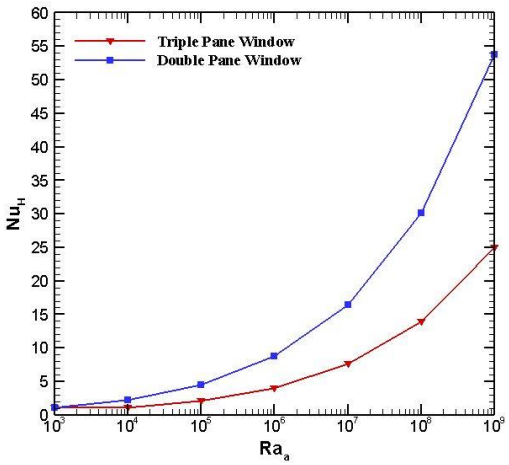

Figure 4.16 Change of Nusselt number with Rayleigh number for double and triple pane window.

4.5 Verification of the physics used

A verification of the physics used with the result of H. Oztop & Bilgen, (2006) is performed assuming conditions as set by H. Oztop & Bilgen (2006) in their computational model. Similarly, a solid wall at constant T_c of h by w is kept at a position c from the hot wall. Results of present study and H. Oztop & Bilgen (2006) are depicted in Figure C1 and Figure C2 in terms of streamline and isothermal plots corresponding to $Ra_{ai} = 10^5$ and 10^6 and $Ra_{ae} = 10^3 – 10^6$. The model is subjected to computational study in COMSOL Multiphysics software.

CHAPTER FIVE: CONCLUSIONS AND RECOMMENDATIONS

5.1 Conclusions

- It is found that the greater the k_r, the better the heat transmission ability. The frequency of wavy partition, on the other hand, has an inverse relationship with thermal exchange performance, with the lower the frequency, the higher the performance. Similarly, the heat transmission performance is less affected by variations in position of the wavy partition.
- The findings show that increasing thermal exchange can be accomplished by selecting partition of higher k_r. Heat transmission, on the other hand, reduces as the thickness and position of the barrier from the cold wall increases. For constant thickness and material, thermal exchange corresponding to the shortest distance of partition wall from the cold end is found to be highest, meaning that the shorter the length of an air-filled chest, the higher the thermal and flow performance.
- Moreover, for the comparative analysis for the thermal exchange performance between the solid and wavy partitioned cavity showed a variation of nearly 8% and 15% corresponding to the enclosure filled without and with the heat generating fluid respectively. The wavy partitioned cavity showed better thermal exchange performance at higher values of Ra.
- Furthermore, the triple pane window showed a reduction of around 50% in thermal exchange performance compared to double paned window.

5.2 Recommendations

- In the realm of conjugate natural convection thermal exchange, there are several potentials. Three dimensional and transient analysis of the present study can provide better insight to thermal performance of enclosures.
- Furthermore, research into the use of nanofluids as the working fluid and their behaviour in a partitioned cavity is possible. The current work used steady-state circumstances, however the time-dependent properties of heat transmission in a partitioned enclosure can be investigated further.

REFRENCES

Acharya, S. (1985). Natural convection in an inclined enclosure containing internal energy sources and cooled from below. *International Journal of Heat and Fluid Flow*, *6*(2), 113–121. https://doi.org/10.1016/0142-727X(85)90045-1

Acharya, S., & Tsang, C. H. (1985). Natural convection in a fully partitioned, inclined enclosure. *Numerical Heat Transfer*, *8*(4), 407–428. https://doi.org/10.1080/01495728508961863

Amgad Salama, M. E. A. and S. S. C. T. P. L., & King Abdullah University of Science and Technology, Jeddah, S. A. (2014). Numerical investigation of natural convection in two enclosures separated by anisotropic solid wall. *International Journal of Numerical Methods for Heat and Fluid Flow*, *24*(4). https://doi.org/10.1108/HFF-02-2014-0034

Anderson, R. E. N., & Bejan, A. (1981). *Vertical Walls in Natural Convection : 24*, 1611–1620.

Cuckovic-Dzodzo, D. M., Dzodzo, M. B., & Pavlovic, M. D. (1999). Laminar natural convection in a fully partitioned enclosure containing fluid with nonlinear thermophysical properties. *International Journal of Heat and Fluid Flow*, *20*(6), 614–623. https://doi.org/10.1016/S0142-727X(99)00053-3

Fusegi, T., Hyun, J. M., & Kuwahara, K. (1992). Natural convection in a differentially heated square cavity with internal heat generation. *Numerical Heat Transfer; Part A: Applications*, *21*(2), 215–229. https://doi.org/10.1080/10407789108944873

Ghosh, P. K., Sarkar, A., & Sastri, V. M. K. (1992). Natural convection heat transfer in an enclosure with a partition - a finite-element analysis. *Numerical Heat Transfer; Part A: Applications*, *21*(2), 231–248. https://doi.org/10.1080/10407789108944874

Hdhiri, N., Souayeh, B., Alfannakh, H., & Beya, B. Ben. (2019). Natural Convection Study with Internal Heat Generation on Heat Transfer and Fluid Flow Within a Differentially Heated Square Cavity Filled with Different Working Fluids and Porous Media. *BioNanoScience*, *9*(3), 702–722. https://doi.org/10.1007/s12668-

019-00626-y

Ho, C. J., & Yih, Y. L. (1987). Conjugate natural convection heat transfer in an air-filled rectangular cavity. *International Communications in Heat and Mass Transfer*, *14*(1), 91–100. https://doi.org/10.1016/0735-1933(87)90011-X

Kahveci, K. (2007a). Natural convection in a partitioned vertical enclosure heated with a uniform heat flux. *Journal of Heat Transfer*, *129*(6), 717–726. https://doi.org/10.1115/1.2717241

Kahveci, K. (2007b). Numerical simulation of natural convection in a partitioned enclosure using PDQ method. *International Journal of Numerical Methods for Heat and Fluid Flow*, *17*(4), 439–456. https://doi.org/10.1108/09615530710739194

Kahveci, K., & Öztuna, S. (2008). A differential quadrature solution of MHD natural convection in an inclined enclosure with a partition. *Journal of Fluids Engineering, Transactions of the ASME*, *130*(2), 0211021–02110214. https://doi.org/10.1115/1.2829567

Kangni, A., Ben Yedder, R., & Bilgen, E. (1991). Natural convection and conduction in enclosures with multiple vertical partitions. *International Journal of Heat and Mass Transfer*, *34*(11), 2819–2825. https://doi.org/10.1016/0017-9310(91)90242-7

Khatamifar, M., Lin, W., Armfield, S. W., Holmes, D., & Kirkpatrick, M. P. (2017). Conjugate natural convection heat transfer in a partitioned differentially-heated square cavity. *International Communications in Heat and Mass Transfer*, *81*, 92–103. https://doi.org/10.1016/j.icheatmasstransfer.2016.12.003

Nishimura, T., Shiraishi, M., Nagasawa, F., & Kawamura, Y. (1988). Natural convection heat transfer in enclosures with multiple vertical partitions. *International Journal of Heat and Mass Transfer*, *31*(8), 1679–1686. https://doi.org/10.1016/0017-9310(88)90280-3

Oztop, H. F., Varol, Y., & Koca, A. (2009). Natural convection in a vertically divided square enclosure by a solid partition into air and water regions. *International Journal of Heat and Mass Transfer*, *52*(25–26), 5909–5921. https://doi.org/10.1016/j.ijheatmasstransfer.2009.07.016

Saha, S. C., Molla, M., Saha, S., & Gu, Y. T. (n.d.). *Natural Convection of Coupled Thermal boundary layers Adjacent to a Wavy Conducting Partition Placed in a Square Di ff erential Heated Enclosure*.

Tong, T. W., & Gerner, F. M. (1986). Natural convection in partitioned air-filled rectangular enclosures. *International Communications in Heat and Mass Transfer*, *13*(1), 99–108. https://doi.org/10.1016/0735-1933(86)90076-X

Turkoglu, H., & Yücel, N. (1996). Natural convection heat transfer in enclosures with conducting multiple partitions and side walls. *Heat and Mass Transfer/Waerme-Und Stoffuebertragung*, *32*(1–2), 1–8. https://doi.org/10.1007/s002310050084

Varol, Y., Oztop, H. F., & Koca, A. (2010). Effects of inclination angle on conduction-natural convection in divided enclosures filled with different fluids. *International Communications in Heat and Mass Transfer*, *37*(2), 182–191. https://doi.org/10.1016/j.icheatmasstransfer.2009.09.016

Williamson, N., Armfield, S. W., & Kirkpatrick, M. P. (2012). Transition to oscillatory flow in a differentially heated cavity with a conducting partition. *Journal of Fluid Mechanics*, *693*(March 2015), 93–114. https://doi.org/10.1017/jfm.2011.471

Xu, F., Patterson, J. C., & Lei, C. (2009). International Journal of Heat and Mass Transfer Heat transfer through coupled thermal boundary layers induced by a suddenly generated temperature difference. *International Journal of Heat and Mass Transfer*, *52*(21–22), 4966–4975. https://doi.org/10.1016/j.ijheatmasstransfer.2009.06.004

APPENDIX A: ISOTHERM AND STREAMLINE PLOTS FOR SOLID PARTITIONED CAVITY

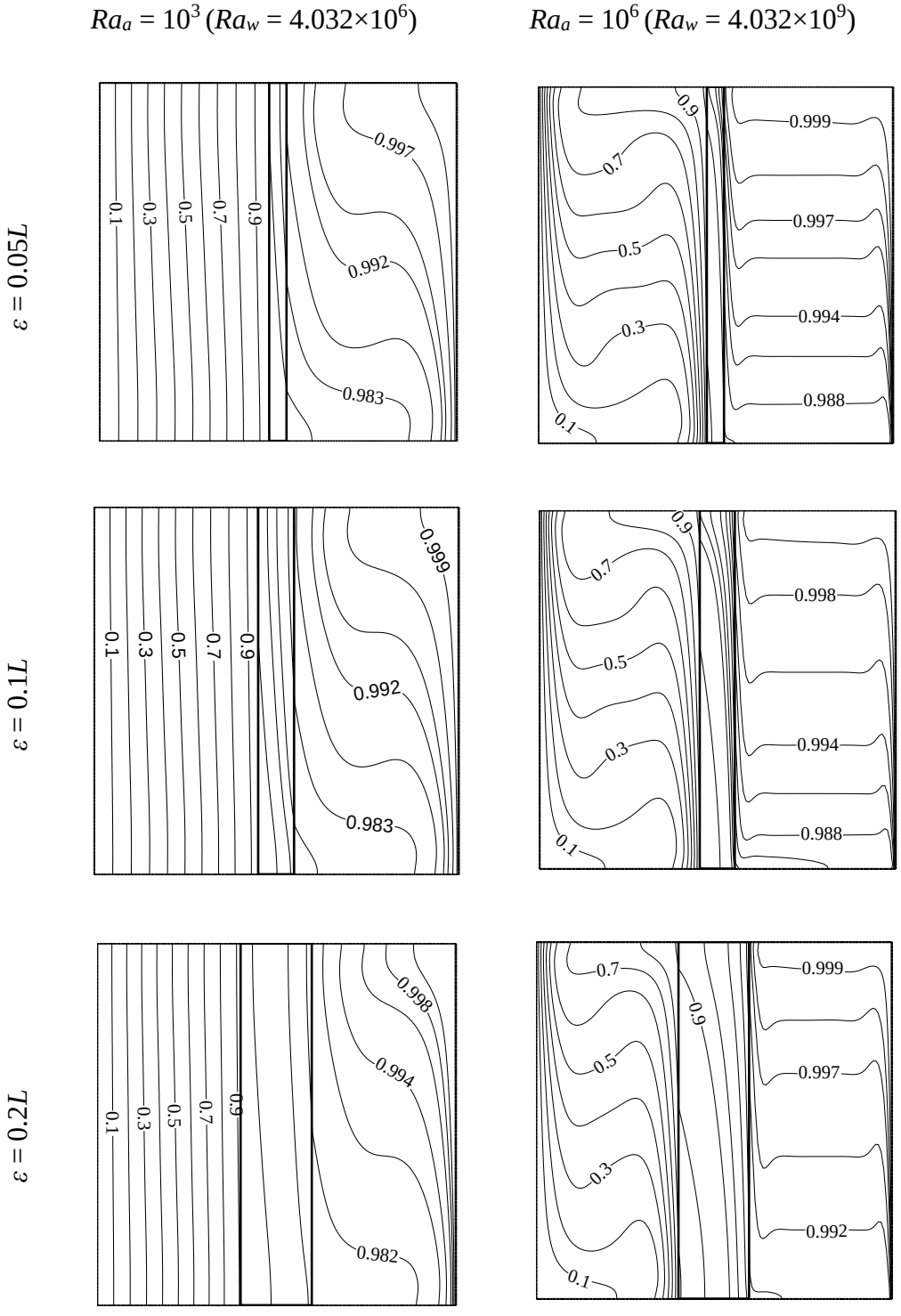

Figure A1 Isothermal contours for $c = 0.50L$ and $k_s = 0.12$ W/m.K, and varying thickness.

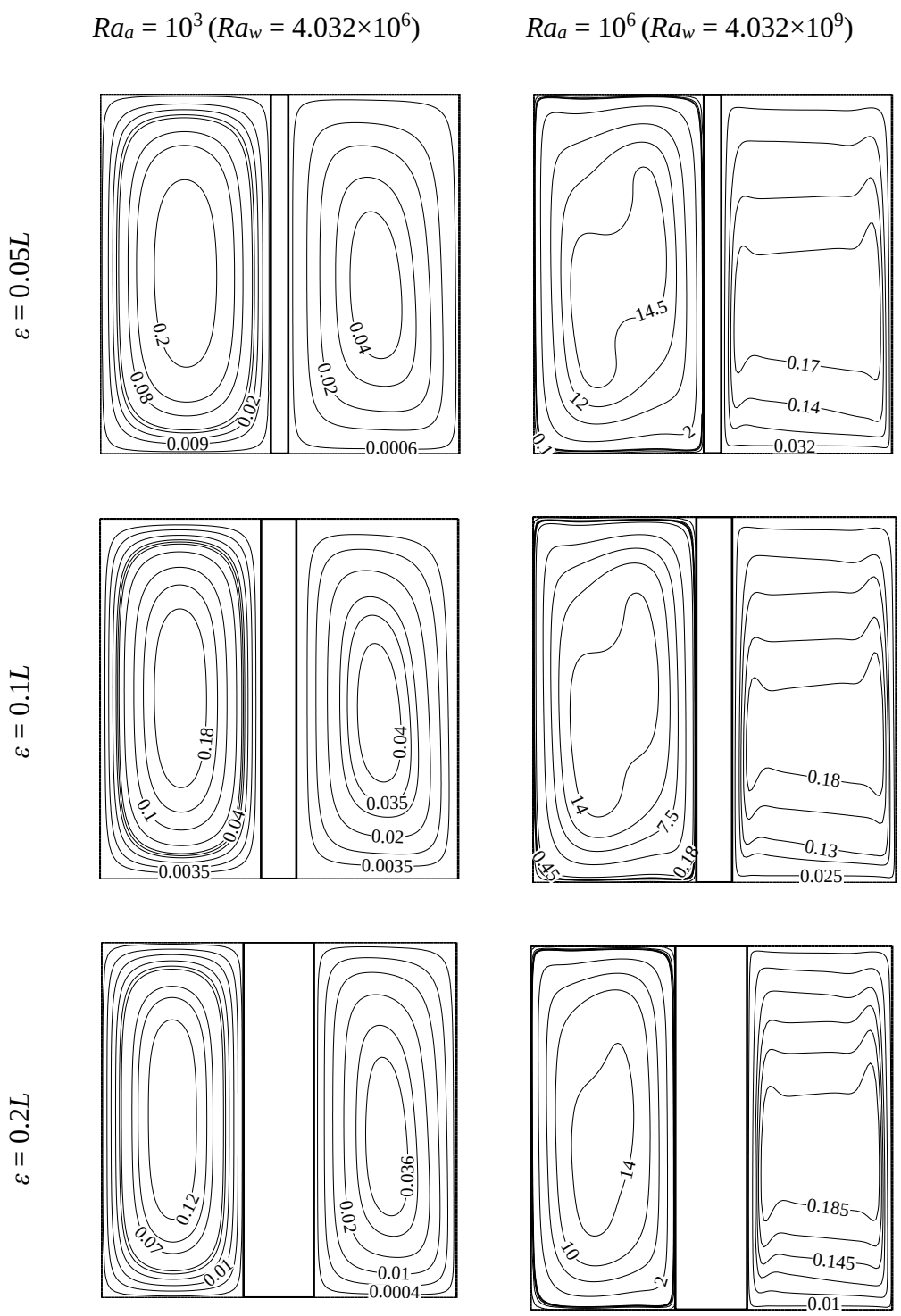

Figure A2 Streamlines for for $c = 0.50L$ and $k_s = 0.12$ W/m.K, and for varying thickness.

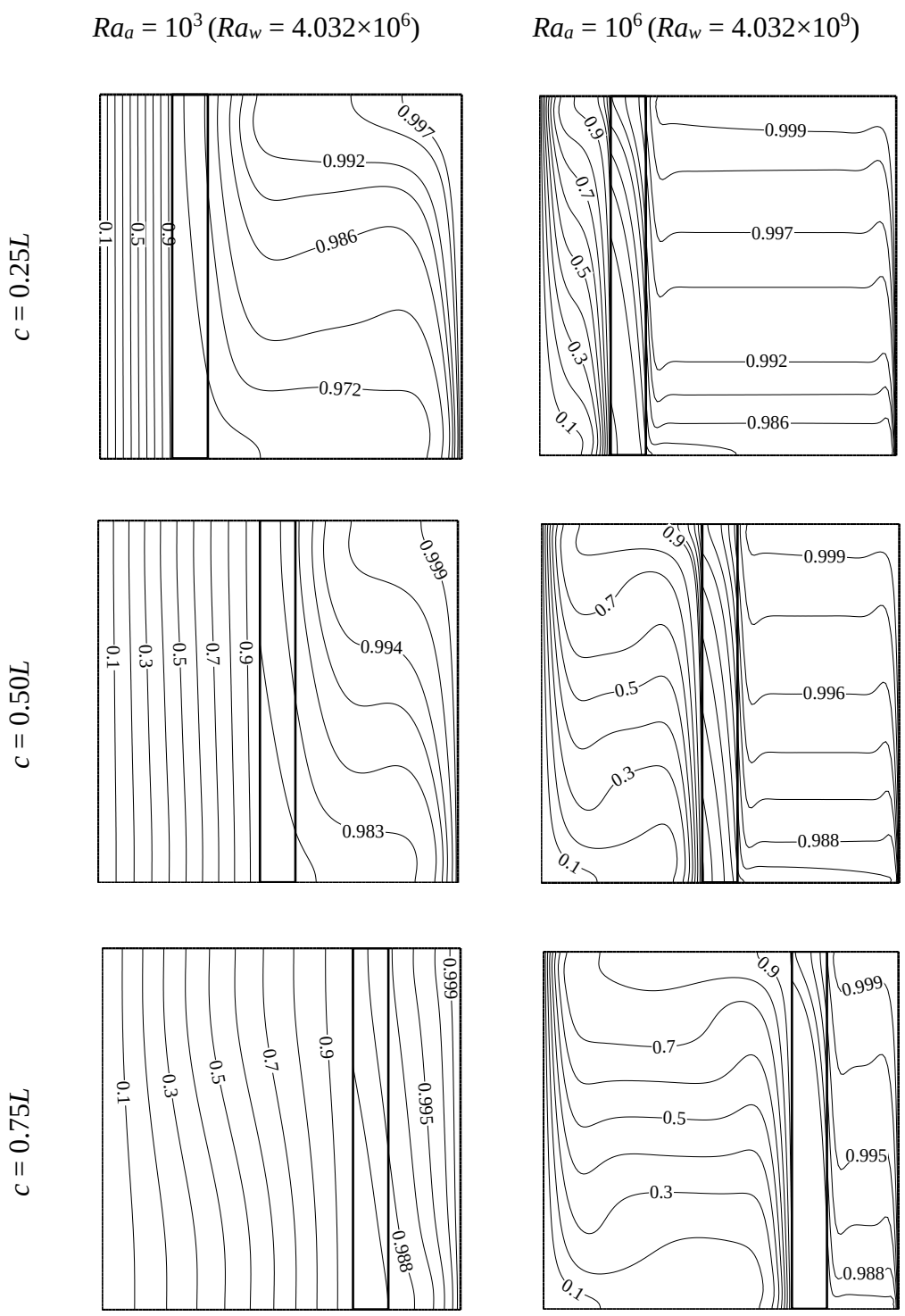

Figure A3 Isothermal contours for $\varepsilon = 0.1L$ and $k_s = 0.72$ W/m.K, for various positions.

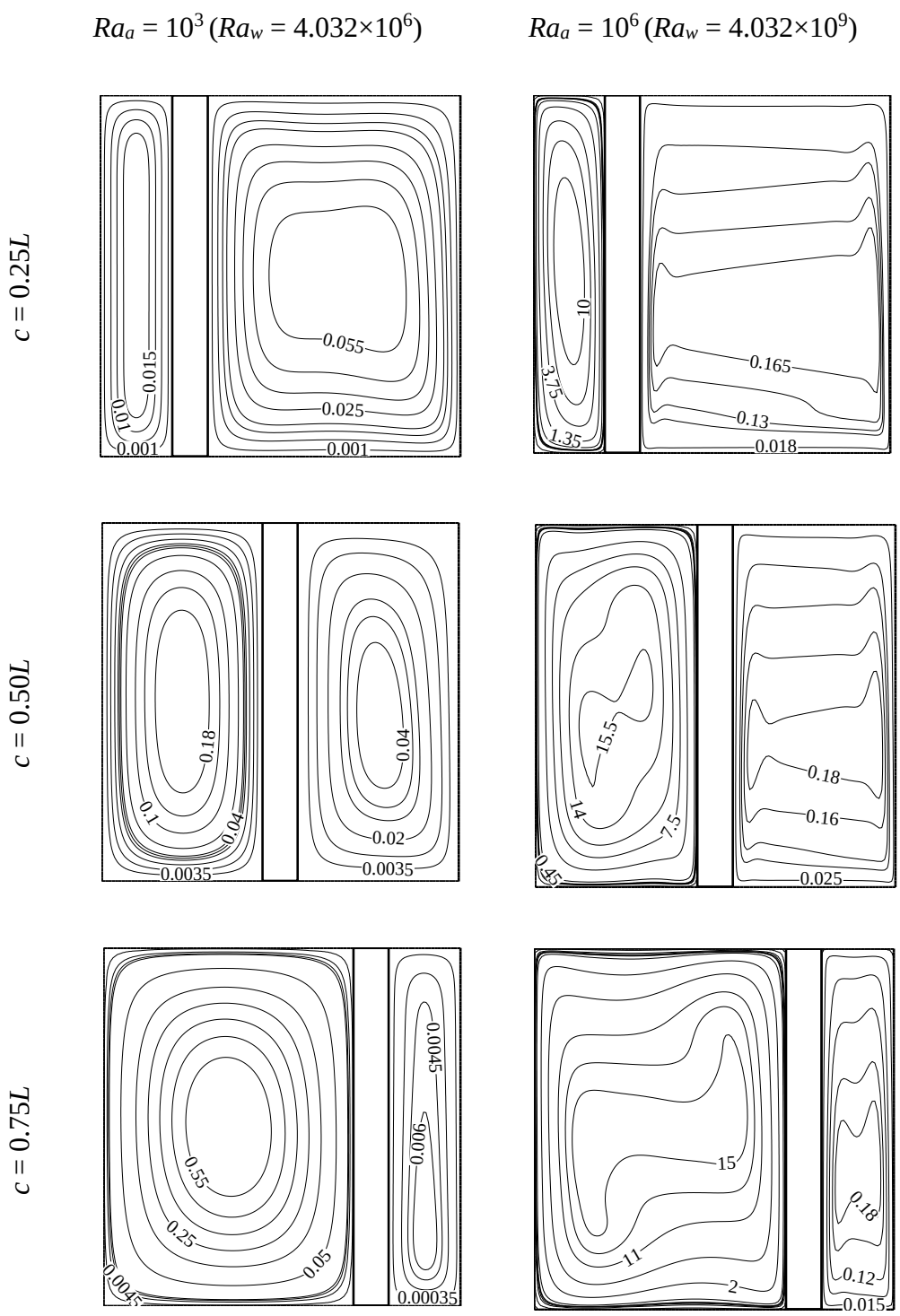

Figure A4 Streamlines for $\varepsilon = 0.1L$ and $k_s = 0.72$ W/m.K, for for various positions.

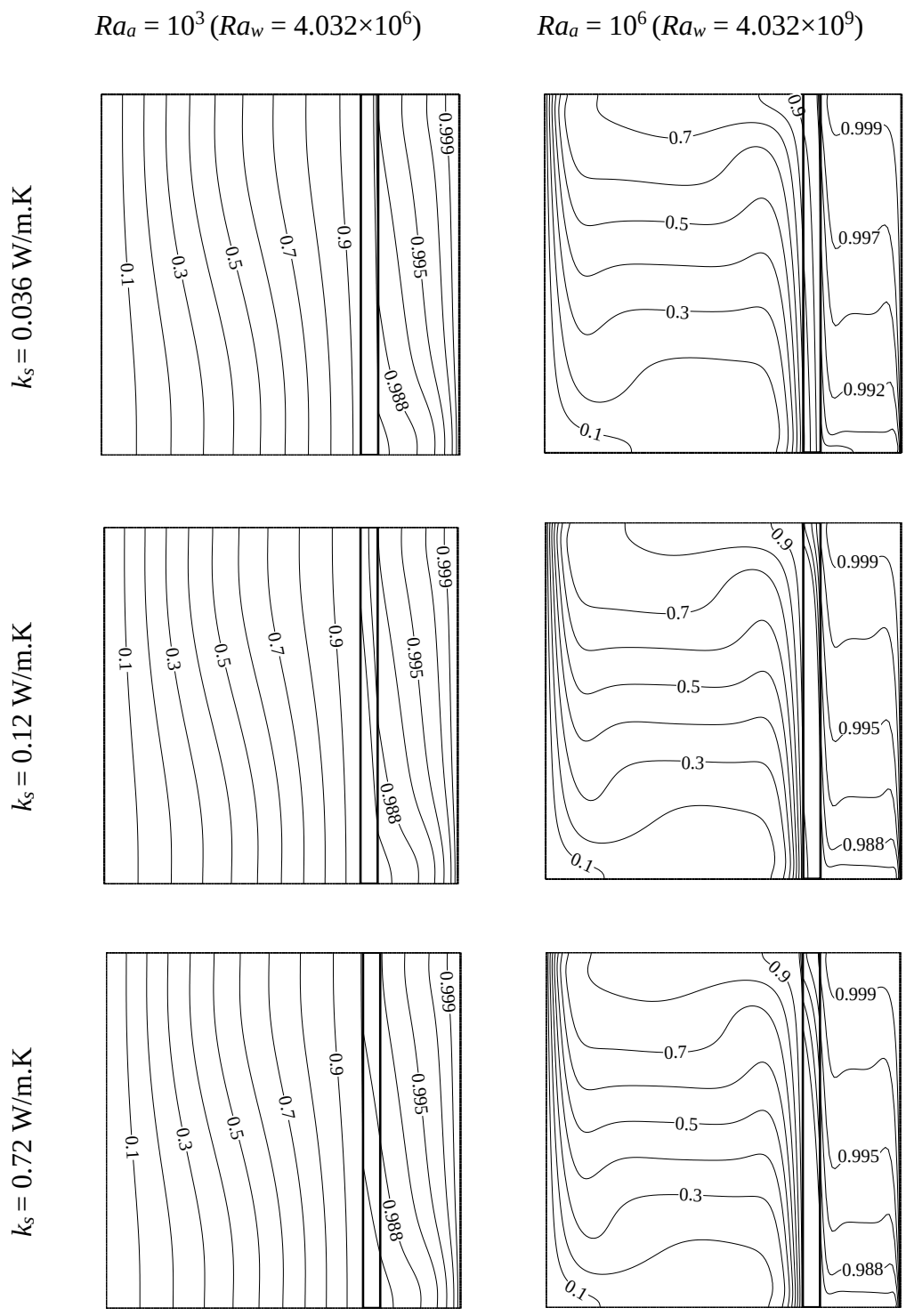

Figure A5 Isothermal contours for $\varepsilon = 0.1L$ and $c = 0.50L$, for various materials.

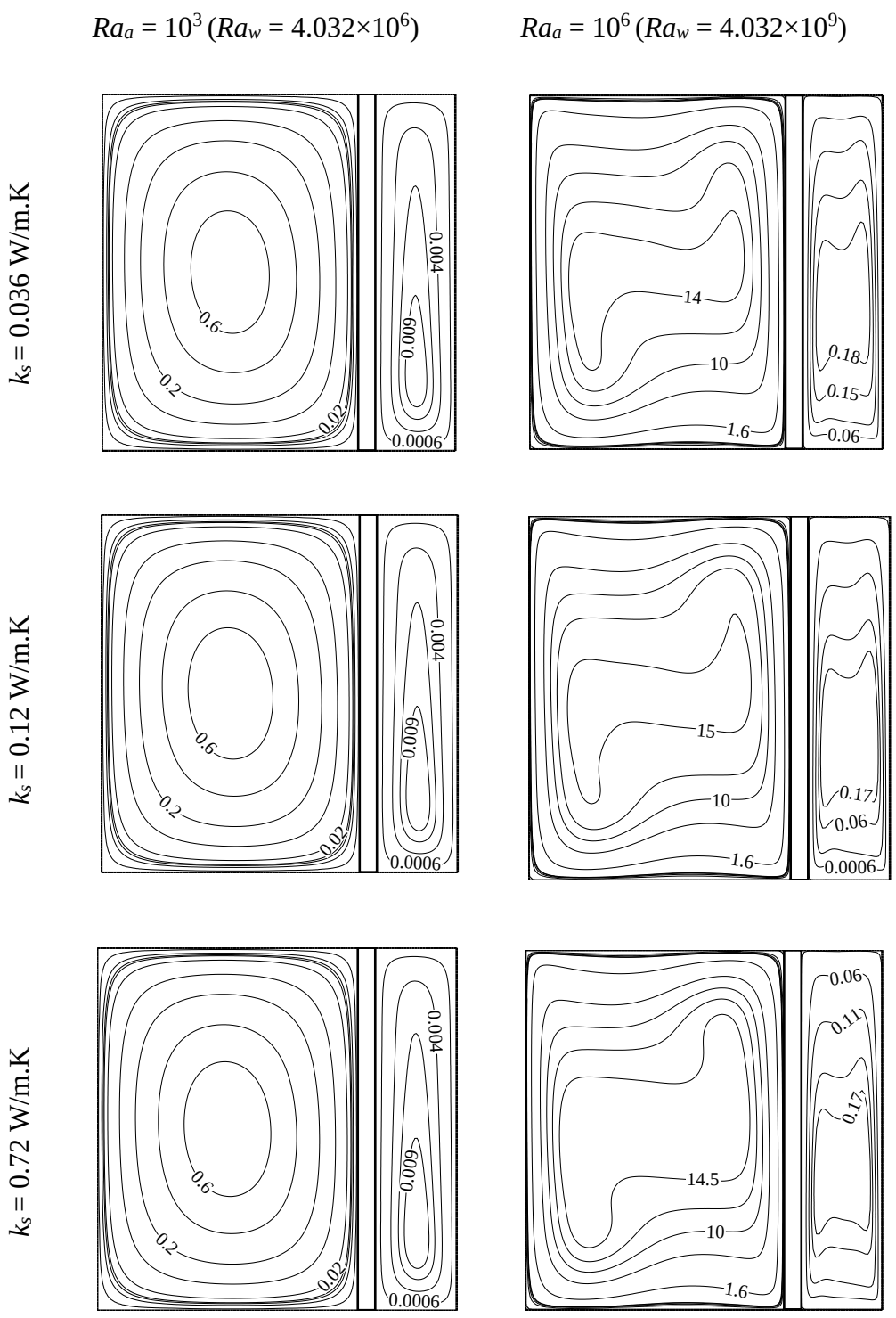

Figure A6 Streamlines for $\varepsilon = 0.1L$ and $c = 0.50L$, for various materials.

APPENDIX B: ISOTHERM AND STREAMLINE PLOTS FOR WAVY PARTITIONED CAVITY

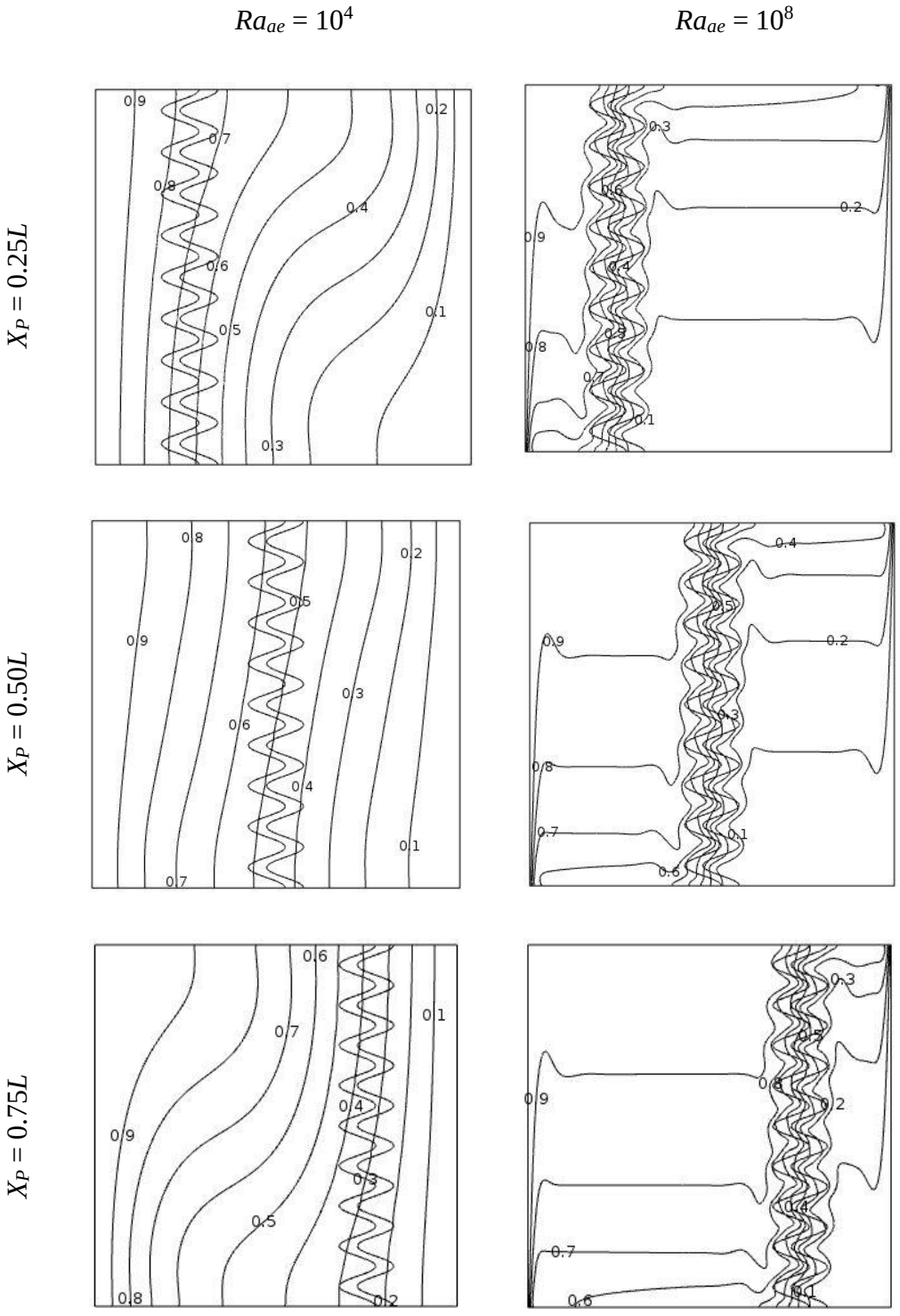

Figure B1 Isothermal contours for $f = 9$ and $k_r = 1.39$, and for various positions.

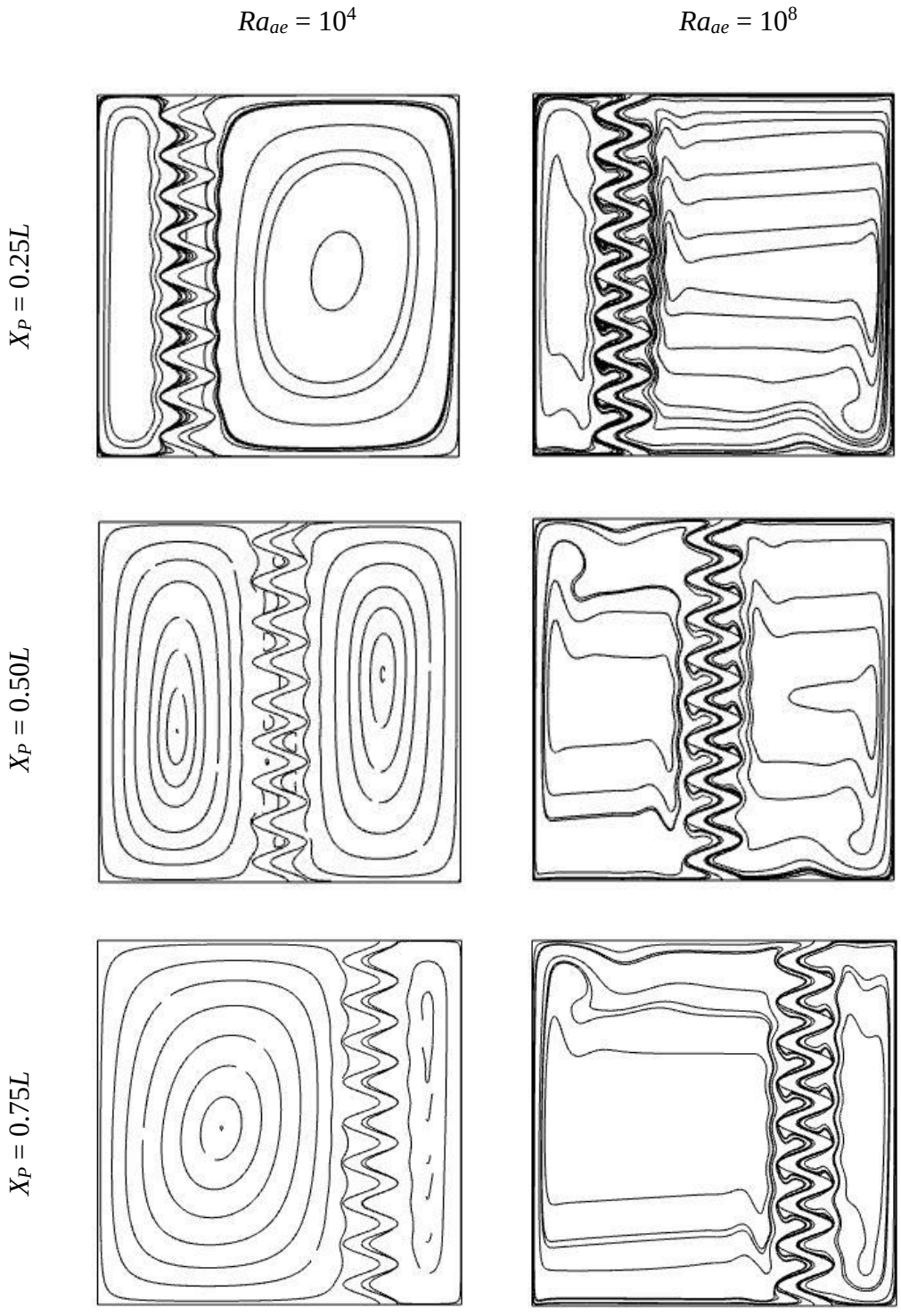

Figure B2 Streamlines for $f = 9$ and $k_r = 1.39$, and for various positions.

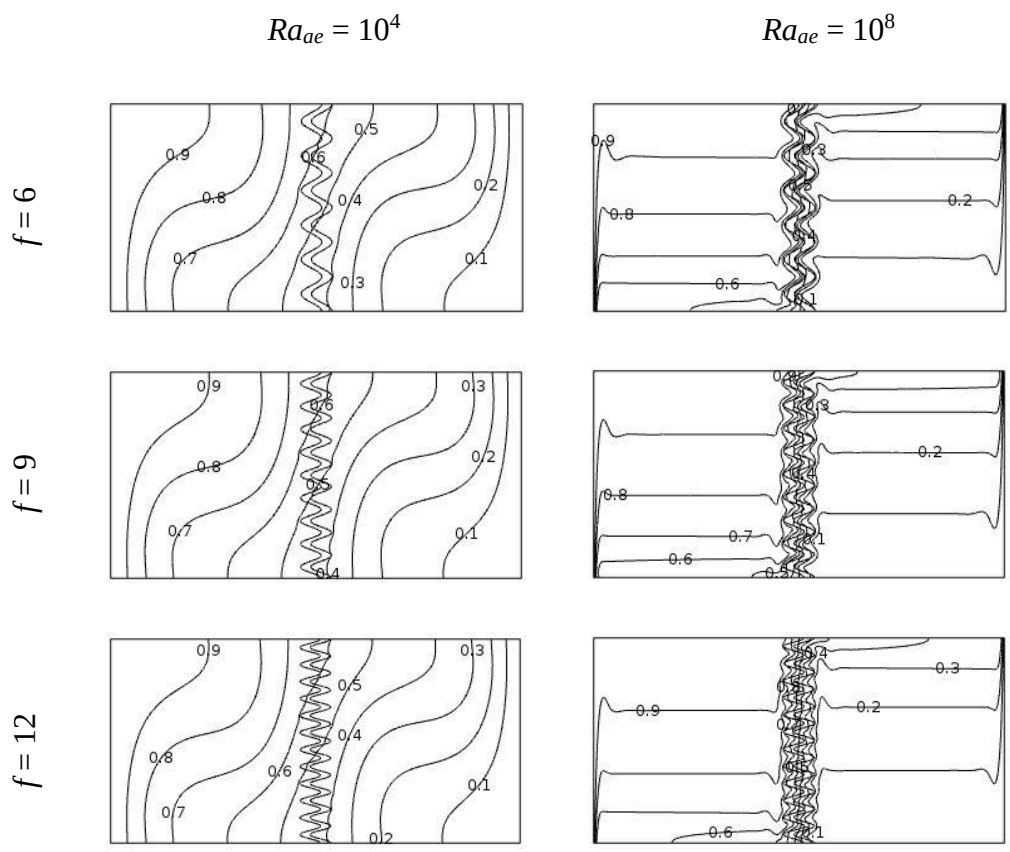

Figure B3 Isothermal contours for $X_p = 0.50L$ and $k_r = 4.63$, for various frequency.

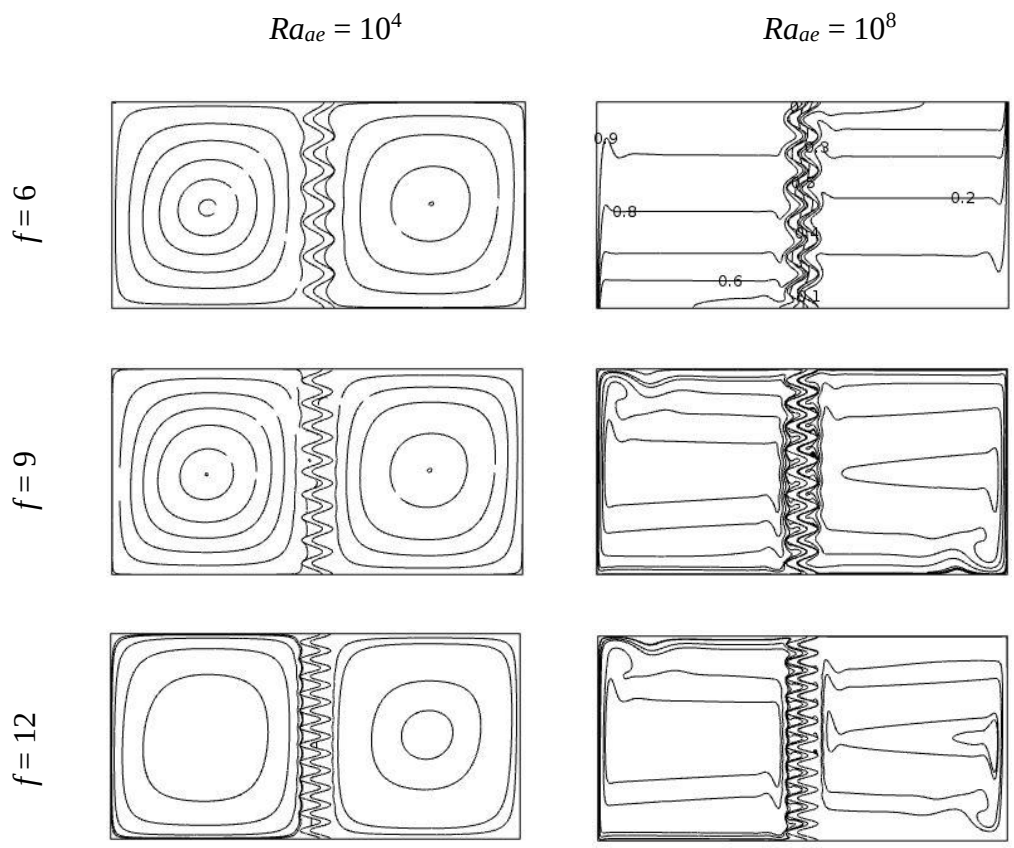

Figure B4 Streamlines for $X_p = 0.50L$ and $k_r = 4.63$, for various frequency.

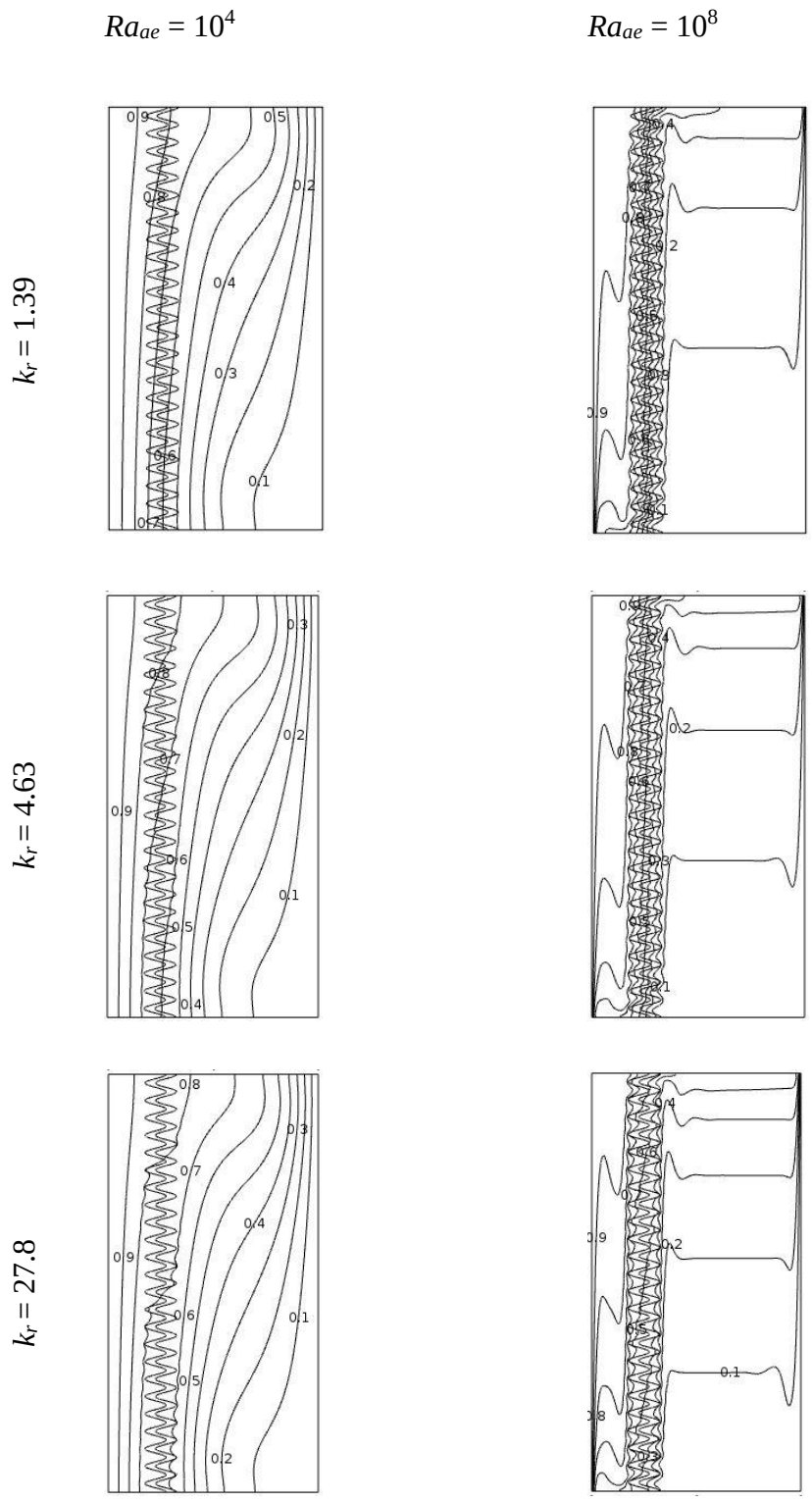

Figure B5 Isothermal contours for $X_p = 0.25L$ and $f = 12$, for various materials.

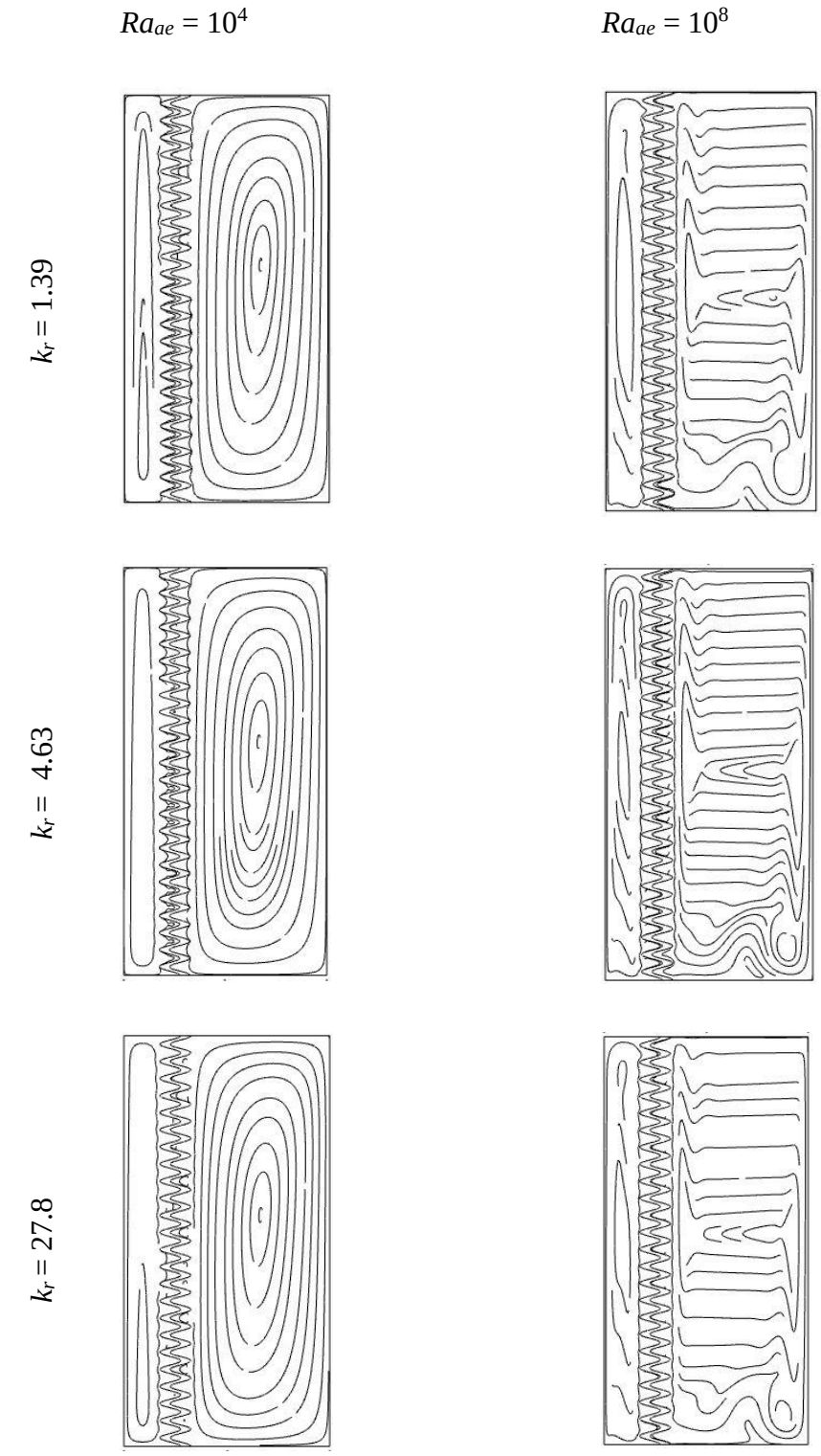

Figure B6 Streamlines for $X_p = 0.25L$ and $f = 12$, for various materials.

APPENDIX C: ISOTHERM AND STREAMLINE PLOTS FOR VERIFICATION OF PHYSICS USED

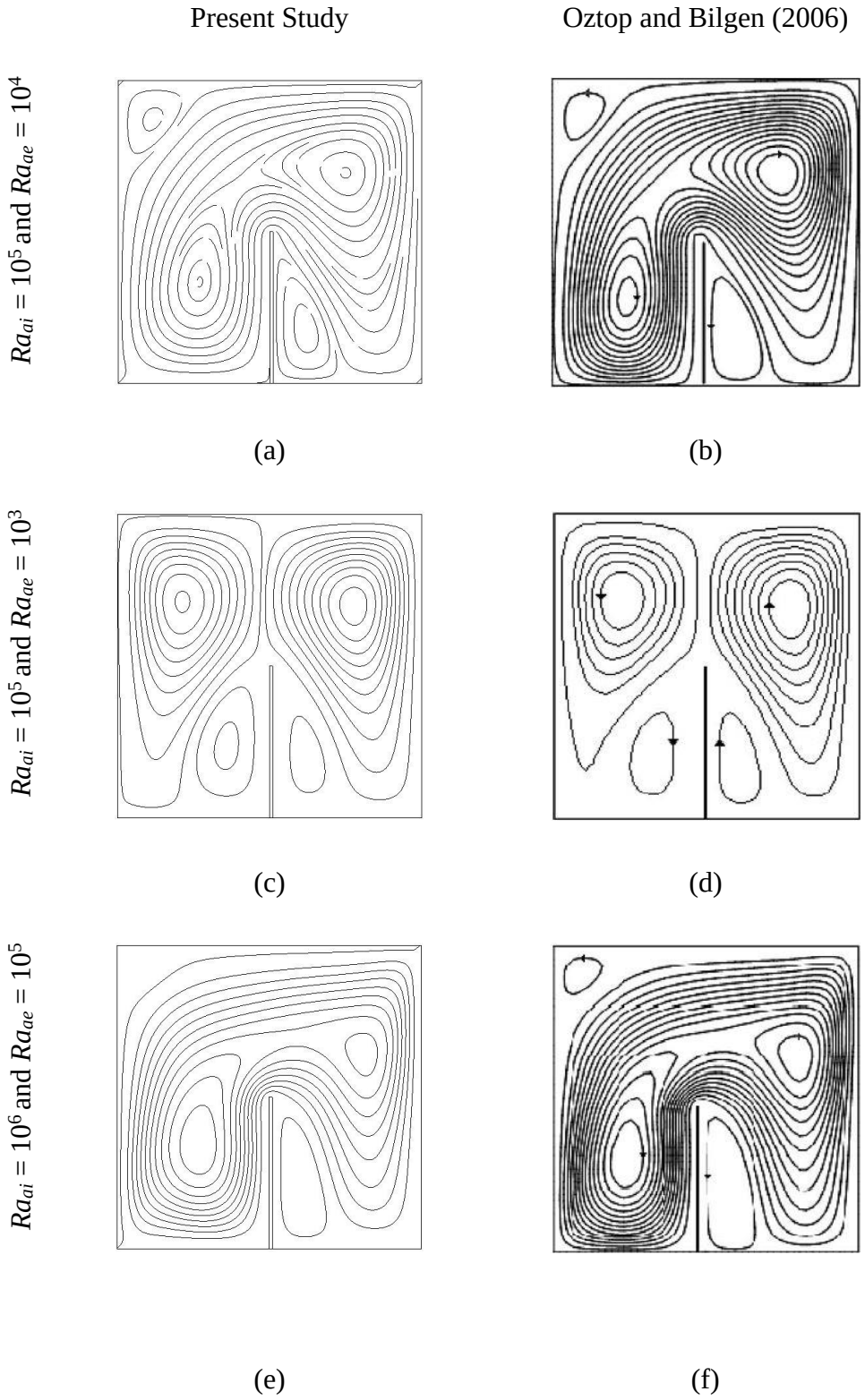

Figure C1 Comparison of streamline plots between the present study and Oztop and Bilgen (2006).

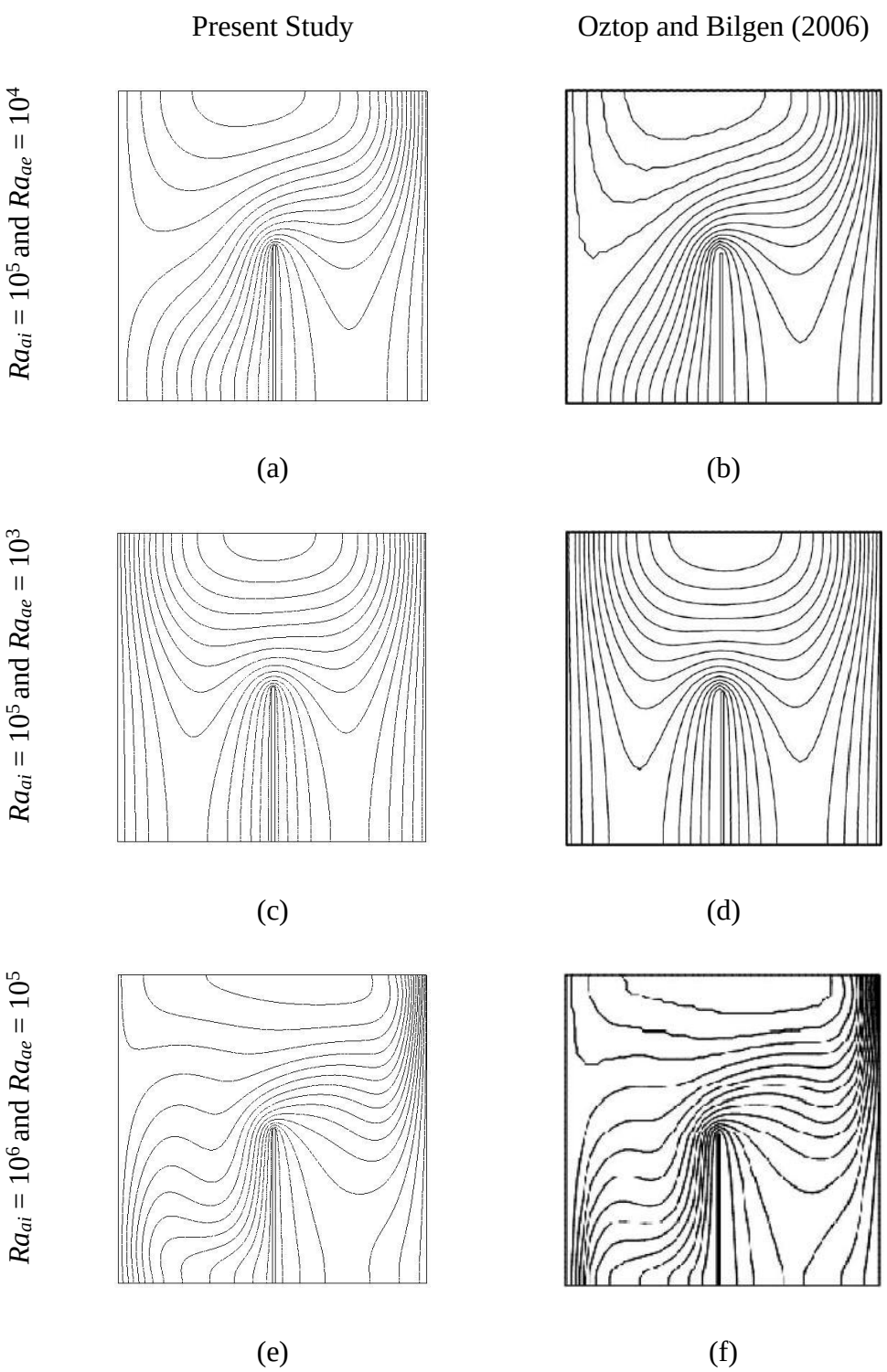

Figure C2 Comparison of isothermal plots between the present study and Oztop and Bilgen (2006).